# Theoretical Design of Open-Shell Singlet Molecular Systems for Nonlinear Optics

Masayoshi Nakano*,[†] and Benoît Champagne[§]

[†]Department of Materials Engineering Science, Graduate School of Engineering Science, Osaka University, Toyonaka, Osaka 560-8531, Japan

[§]Laboratoire de Chimie Théorique, University of Namur, rue de Bruxelles, 61, 5000 Namur, Belgium

**ABSTRACT:** Design principles toward open-shell singlet molecular systems exhibiting remarkable nonlinear optical (NLO) responses are derived based on a two-site diradical model within the valence configuration interaction scheme. In this scheme, the concept of diradical character ($y$), a chemical index for bond weakness in the ground state, enables to classify singlet molecular systems into three categories: (i) closed-shell ($y = 0$), (ii) intermediate diradical ($0 < y < 1$), and (iii) pure open-shell ($y = 1$) systems. It is found that the second hyperpolarizabilities (and also the first hyperpolarizabilities for asymmetric systems) are enhanced in the intermediate diradical character region with respect to the other ones. This leads to a new class of open-shell singlet NLO systems, which are expected to outstrip traditional closed-shell NLO systems. On the basis of this principle, practical molecular design guidelines for tuning the diradical characters and, therefore, for achieving large NLO properties are discussed on the basis of first-principles calculations performed on realistic open-shell singlet molecular systems.
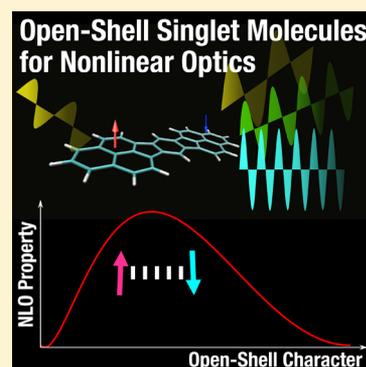
Over four decades, nonlinear optical (NLO) phenomena, which result from the interactions between atoms/molecules and strong electric fields like lasers, have attracted a great deal of attention from experimental and theoretical researchers due to their numerous applications in spectroscopy, materials science, and engineering.[1−4] In particular, NLO active materials are expected to be utilized in future photonics, that is, data acquisition, storage, processing, and transmission by photons,[5−15] so that intense research activities have been devoted to prepare highly active NLO molecules with large first ($\beta$) and second ($\gamma$) hyperpolarizabilities. Although conventional NLO materials are generally inorganic crystals, for example, lithium niobate ($LiNbO_3$) and potassium dihydrogen phosphate ($KH_2PO_4$), and exhibit second harmonic generation (SHG), since the 1990s, $\pi$-electron conjugated organic molecular systems have appeared as promising alternatives for highly efficient NLO applications[1−4] because of their larger optical nonlinearities and faster optical responses as well as of lower driving voltages, easier molecular design, and potentially lower processing cost. So far, many organic $\pi$-conjugated molecular systems have been investigated, and several design guidelines for preparing efficient NLO molecules have been proposed, for example, $\pi$-conjugation extension,[16] donor/acceptor group substitution,[17,18] and charge introduction.[19] However, most of these systems are closed-shell systems, whereas there have been few studies on open-shell systems, in particular, open-shell singlet systems, before our investigations.

Open-shell singlet systems, $n$-radicals/$n$-radicaloids ($n = 2$ (di), 4 (tetra), 6 (hexa), ...),[20−32] are defined as "systems having $n$ weakly interacting electrons with similar energy". In the molecular orbital (MO) picture, they are also represented as "systems with $n$ nearly degenerate bonding and antibonding

MOs". For example, the stretched hydrogen molecule and the twisted ethylene are prototypical models for diradical systems,[20] where the degree of diradical character, that is, bond weakness in this case, is controlled by the degree of the structural changes. Although such model systems are thermally unstable or are observed as reaction intermediates with short lifetimes,[29] recent development in synthesis have led to various types of thermally stable diradicaloids and multiradicaloids, for example, diphenalenyl compounds,[33,34] transition metal compounds,[35−37] polycyclic aromatic hydrocarbons (PAHs),[29,30,38,39] and main group containing compounds.[24,40−42] These open-shell singlet systems exhibit unique physicochemical properties, for example, the narrow singlet−triplet band gap (∼0.5 eV) in long acenes having a singlet ground state and a high reactivity of the zigzag edges,[43−45] high charge carrier mobilities,[33] and in the solid state, intermolecular distances smaller than van der Waals radius.[33,46] These unique properties originate from their unique electronic structures, which can be characterized by the open-shell or multiradical character.[31,47−51] The diradical (and higher order) character is not an observable, but a quantum-chemical index, which was originally defined as twice the weight of the double excitation configuration in the multiconfiguration self-consistent-field (MC-SCF) method.[47] Yamaguchi proposed an approximate spin projection scheme for evaluating the diradical character ($y$) using broken symmetry (BS) single-determinant approaches, that is, spin-unrestricted Hartree−Fock (UHF) and density functional theory (UDFT) methods.[31,48] Subsequently,
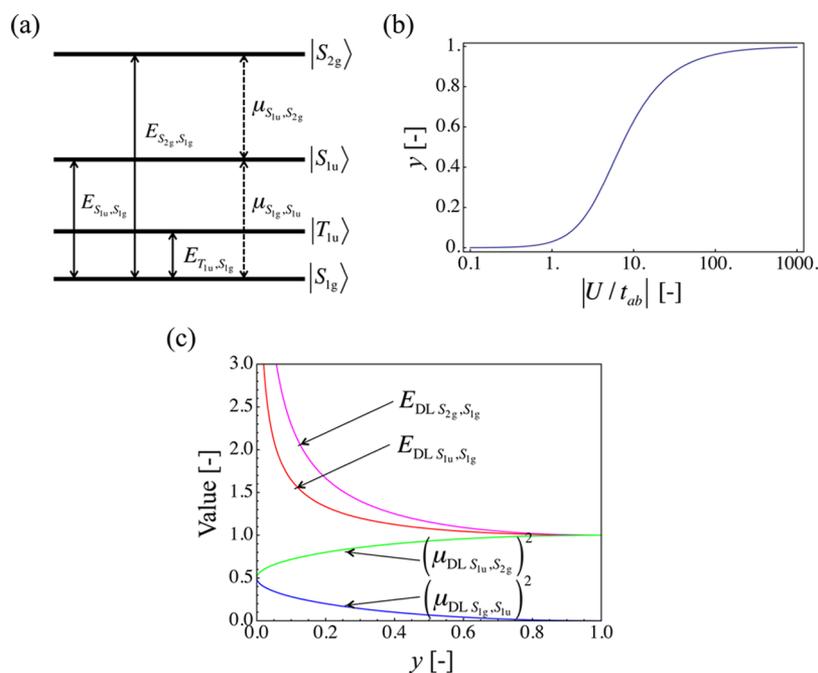
**Figure 1.** Four states $\{|S_{1g}\rangle, |T_{1u}\rangle, |S_{1u}\rangle, |S_{2g}\rangle\}$ of the two-site diradical model (a), diradical character $y$ versus $|U/t_{ab}|$ (b), as well as diradical character dependences of dimensionless excitation energies ($E_{DL\ S_{1u},S_{1g}}$ and $E_{DL\ S_{2g},S_{1g}}$), squared transition moments (($\mu_{DL\ S_{1g},S_{1u}}$)$^2$, and ($\mu_{DL\ S_{1u},S_{2g}}$)$^2$) (c).

the diradical character was associated with the "instability of chemical bonds in the ground state".[31] On the other hand, excitation energies and other molecular properties are also strongly related to the diradical character in the ground state.[20,22,32,52−54] So, analytical expressions have been derived for the excitation energies and transition moments as a function of the diradical character using a two-site diradical model based on the valence configuration interaction (2e-VCI) method.[53] Because the diradical character is a chemical index, related to the effective bond nature in the ground state and, thus, is familiar to chemists, such expressions are useful for deducing design guidelines for efficient photoresponsive molecular systems.[32]

The electronic structure of open-shell singlet systems is classified into three categories, that is, (i) closed-shell ($y = 0$), (ii) intermediate diradical ($0 < y < 1$), and (iii) pure open-shell ($y = 1$) systems.[32] On the basis of theoretical and computational studies, we have found that $\gamma$, the third-order NLO property at the molecular scale, shows a strong correlation with the diradical character $y$, referred to as "$y-\gamma$ correlation": systems having intermediate $y$ values around 0.5 exhibit larger $\gamma$ amplitudes than closed-shell ($y = 0$) and pure diradical ($y = 1$) systems of similar molecular sizes.[55] The $y-\gamma$ correlation was clarified using analytical expressions derived from the 2e-VCI approach.[53] It was also exemplified using highly correlated ab initio molecular orbital (MO) and spin-unrestricted density functional theory (UDFT) calculations for various model and real open-shell molecular systems, for example, $H_2$ molecule under dissociation,[56,57] twisted ethylene,[55] $p$-quinodimethane,[55] imidazole and triazole benzenes,[58] polycyclic hydrocarbons including graphene nanoflakes,[59−65] multinuclear transition-metal complexes,[66−68] thiophene-based systems,[69] main group compounds,[70−72] and photochromic compounds.[73] Such diradical character dependence of $\gamma$ subsequently has been confirmed experimentally by remarkably large two-photon absorption (TPA)[74−81] and third harmonic generation (THG), which are typical third-order NLO properties, of several thermally stable open-shell singlet diradicaloids,[82,83] having intermediate $y$ values. Further extension

of the diradical character dependence of $\gamma$ has been observed for multiradical systems,[84−89] asymmetric open-shell singlet systems,[90−92] dynamic NLO (resonant NLO including TPA) properties,[93] and other linear and nonlinear optical properties including $\beta$.[90] In this Perspective, we explain the theoretical background of this novel design principle toward enhanced NLO properties and give examples of realistic open-shell singlet NLO molecular systems with intermediate $y$ values.

*Symmetric Open-Shell Singlet Systems.* First, we consider the excitation energies and properties of diradical molecules as a function of diradical character. The simplest model for symmetric diradical molecules consists in a two-site model A•−B• with two electrons in two orbitals. The localized natural orbitals (LNOs) are defined by using symmetry-adapted bonding ($g$) and antibonding ($u$) orbitals[22,52,53]

$$a(x) \equiv \frac{1}{\sqrt{2}}[g(x) + u(x)] \text{ and } b(x) \equiv \frac{1}{\sqrt{2}}[g(x) - u(x)] \tag{1}$$

which are localized on one site (A or B), whereas they have generally small tails on the other site, satisfying the orthogonal condition, $\langle a|b\rangle = 0$. $M_S$, the $z$ component of spin angular momentum is equal to 0 (singlet and triplet). $a$ and $b$ enable to define two neutral and two ionic determinants

$$|a\bar{b}\rangle \equiv |\text{core } a\bar{b}\rangle \text{ and } |\bar{b}a\rangle \equiv |\text{core } \bar{b}a\rangle \qquad \text{(neutral)} \tag{2a}$$

$$|a\bar{a}\rangle \equiv |\text{core } a\bar{a}\rangle \text{ and } |b\bar{b}\rangle \equiv |\text{core } b\bar{b}\rangle \qquad \text{(ionic)} \tag{2b}$$

Here, the upper-bar indicates the beta spin, whereas nonbar does the alpha spin. The electronic Hamiltonian $H$ (in atomic units) reads

$$H = -\frac{1}{2}\sum_{i=1}^{N}\nabla_i^2 - \sum_{i=1}^{N}\sum_{A=1}^{2}\frac{Z_A}{r_{iA}} + \sum_{i=1}^{N}\sum_{j>i}^{N}\frac{1}{r_{ij}}$$

$$= \sum_{i=1}^{N}h(i) + \sum_{i=1}^{N}\sum_{j>i}^{N}\frac{1}{r_{ij}} \qquad (3)$$

In this basis, the VCI matrix of this Hamiltonian is given by[52,53]

$$\begin{pmatrix} \langle a\bar{b}|H|a\bar{b}\rangle & \langle a\bar{b}|H|b\bar{a}\rangle & \langle a\bar{b}|H|a\bar{a}\rangle & \langle a\bar{b}|H|b\bar{b}\rangle \\ \langle b\bar{a}|H|a\bar{b}\rangle & \langle b\bar{a}|H|b\bar{a}\rangle & \langle b\bar{a}|H|a\bar{a}\rangle & \langle b\bar{a}|H|b\bar{b}\rangle \\ \langle a\bar{a}|H|a\bar{b}\rangle & \langle a\bar{a}|H|b\bar{a}\rangle & \langle a\bar{a}|H|a\bar{a}\rangle & \langle a\bar{a}|H|b\bar{b}\rangle \\ \langle b\bar{b}|H|a\bar{b}\rangle & \langle b\bar{b}|H|b\bar{a}\rangle & \langle b\bar{b}|H|a\bar{a}\rangle & \langle b\bar{b}|H|b\bar{b}\rangle \end{pmatrix}$$

$$= \begin{pmatrix} 0 & K_{ab} & t_{ab} & t_{ab} \\ K_{ab} & 0 & t_{ab} & t_{ab} \\ t_{ab} & t_{ab} & U & K_{ab} \\ t_{ab} & t_{ab} & K_{ab} & U \end{pmatrix} \qquad (4)$$

where the energy of the neutral determinants $\langle a\bar{b}|H|a\bar{b}\rangle (= \langle b\bar{a}|H|b\bar{a}\rangle) = 0$ is taken as the energy origin, and the physical parameters are defined by

$$U \equiv U_{aa} - U_{ab} \equiv (aa|aa) - (aa|bb)$$

(effective Coulomb repulsion) $\qquad (5a)$

$$K_{ab} = K_{ba} \equiv (ab|ba) = (ba|ab) = (ab|ab) = (ba|ba)$$

(direct exchange integral) $\qquad (5b)$

and

$$t_{ab} = t_{ba} \equiv \langle a|f|b\rangle = \langle b|f|a\rangle = \langle \bar{a}|f|\bar{b}\rangle = \langle \bar{b}|f|\bar{a}\rangle$$

(transfer integral) $\qquad (5c)$

where $(ij|kl)$ represents a two-electron integral and $f$ indicates the Fock operator in the LNO basis.[52–54] By diagonalizing the VCI matrix, we obtain four solutions: an essentially neutral lowest-energy singlet state of g symmetry $|S_{1g}\rangle (= \kappa(|a\bar{b}\rangle + |b\bar{a}\rangle) + \eta(|a\bar{a}\rangle + |b\bar{b}\rangle))$ (with energy $^1E_{1g}$; $\kappa > \eta > 0$), an ionic singlet state with u symmetry $|S_{1u}\rangle = (|a\bar{a}\rangle - |b\bar{b}\rangle)/\sqrt{2}$ (with energy $^1E_{1u}$), another singlet state of g symmetry but essentially ionic $|S_{2g}\rangle (= -\eta(|a\bar{b}\rangle + |b\bar{a}\rangle) + \kappa(|a\bar{a}\rangle + |b\bar{b}\rangle))$ (with energy $^1E_{2g}$; $\kappa > \eta > 0$) and a neutral triplet state $|T_{1u}\rangle (= (|a\bar{b}\rangle - |b\bar{a}\rangle)/\sqrt{2}$ (with energy $^3E_{1u}$)[52,53] (see Figure 1a). The nonzero transition moments between these states are evaluated as[53]

$$\mu_{S_{1g},S_{1u}} \equiv -\langle S_{1g}|\sum_i r_i|S_{1u}\rangle = \sqrt{2}\eta R_{BA}$$

and

$$\mu_{S_{2g},S_{1u}} \equiv -\langle S_{2g}|\sum_i r_i|S_{1u}\rangle = \sqrt{2}\kappa R_{BA} \qquad (6)$$

where $R_{BA} = (b|r_1|b) - (a|r_1|a)$ represents the effective distance between the unpaired electrons, and therefore a dipole (when multiplied by the electron charge). $2\kappa^2$ and $2\eta^2$, the sum of which is equal to one by virtue of the orthogonalization condition, are the weights of the neutral (ionic) and ionic (neutral) contributions in $|S_{1g}\rangle$ $(|S_{2g}\rangle)$. In order to elucidate the relationship between the physical parameters $(t_{ab}, U, K_{ab})$ and the ground-state magnetic interaction, we introduce the effective exchange integral $J$ in the Heisenberg Hamiltonian[94] for two-site systems, $\hat{H}_{HB} = -2J\hat{S}_A\cdot\hat{S}_B$, which is expressed by[52,53]

$$2J = {}^1E_{1g} - {}^3E_{1u} = 2K_{ab} + \frac{U - \sqrt{U^2 + 16t_{ab}^2}}{2} \qquad (7)$$

Alternative expressions can be derived using the symmetry-adapted MOs. The g-symmetry ground and excited states are given by $|S_{1g}\rangle = \xi|g\bar{g}\rangle - \zeta|u\bar{u}\rangle$ and $|S_{2g}\rangle = \zeta|g\bar{g}\rangle + \xi|u\bar{u}\rangle$, respectively, where $\xi^2 + \zeta^2 = 1$, and $\xi + \zeta = 2\kappa$ and $\xi - \zeta = 2\eta$ from the comparison of the MO and LNO representations of the wave functions. Following ref 47, $y$ is defined by twice the weight of the double excitation configuration in the singlet ground state so that[53]

$$y \equiv 2\zeta^2$$

$$= 1 - \frac{4|t_{ab}|}{\sqrt{U^2 + 16t_{ab}^2}}$$

$$= 1 - \frac{4r_t}{\sqrt{1 + 16r_t^2}}$$

$$= 1 - \frac{2\sqrt{(r_K - r_J)(r_K - r_J + 1)}}{1 + 2(r_K - r_J)} \qquad (8)$$

using dimensionless quantities: $r_t \equiv |t_{ab}|/U \,(\geq 0)$, $r_K \equiv 2K_{ab}/U$ $(\geq 0)$ and $r_J \equiv 2J/U$. As seen from this equation, the diradical character $y$ satisfies the relations: $y \to 1$ for $r_t \to 0$, and $y \to 0$ for $r_t \geq 1$. These relations ensure that $y$ takes a value between 0 and 1, which represent the closed-shell (bonding) and pure diradical (bond breaking) states, respectively. Because $U$ describes the difficulty of electron transfer between A and B, whereas $|t_{ab}|$ does the easiness of that, the case $r_t \to 0$ defines the localization limit with an electron on each site, corresponding to pure diradical state $(y \to 1)$, whereas the case $r_t \geq 1$ $(|t_{ab}| \geq U)$ represents a significant delocalization of electrons over the two sites, corresponding to stable bonding state $(y \to 0)$ (see Figure 1b). In other words, $y$ is associated with electron correlation through $r_t$. Alternatively, $y$ can be expressed by the occupation number of the lowest unoccupied natural orbital (LUNO), $n_{LUNO}$. Since $n_{LUNO} = 2 - n_{HONO}$, $q = 1 - y = (n_{HONO} - n_{LUNO})/2$ corresponds to an "effective bond order", where $n_{HONO}$ and $n_{LUNO}$ are the numbers of electrons in bonding and antibonding orbitals, respectively. Thus, the diradical character $y$ is a fundamental factor for describing electronic states, that is, $y$ represents an electron correlation in the physical sense and $1 - y$ represents an effective bond order in the chemical sense.[31,32,53,56]

> The diradical character $y$ is a fundamental factor for describing electronic states, that is, $y$ represents an electron correlation in the physical sense and $1 − y$ represents an effective bond order in the chemical sense.

As a matter of fact, the dimensionless (DL) excitation energies and squares of the transition moments are almost fully governed by $q$:[53]

$$E_{\mathrm{DL}\,S_{1u},S_{1g}} \equiv \frac{{}^{1}E_{1u} - {}^{1}E_{1g}}{U}$$

$$= 1 - r_J$$

$$= \frac{1}{2}\left(1 - 2r_K + \frac{1}{\sqrt{1-q^2}}\right) \tag{9a}$$

$$E_{\mathrm{DL}\,S_{2g},S_{1g}} \equiv \frac{{}^{1}E_{2g} - {}^{1}E_{1g}}{U} = 1 + 2(r_K - r_J) = \frac{1}{\sqrt{1-q^2}} \tag{9b}$$

$$(\mu_{\mathrm{DL}\,S_{1g},S_{1u}})^2 \equiv \left(\frac{\mu_{S_{1g},S_{1u}}}{R_{\mathrm{BA}}}\right)^2$$

$$= \frac{r_K - r_J}{1 + 2(r_K - r_J)}$$

$$= \frac{1 - \sqrt{1-q^2}}{2} \tag{9c}$$

and

$$(\mu_{\mathrm{DL}\,S_{1u},S_{2g}})^2 \equiv \left(\frac{\mu_{S_{1u},S_{2g}}}{R_{\mathrm{BA}}}\right)^2$$

$$= \frac{1}{2}\left(1 + \frac{1}{1 + 2(r_K - r_J)}\right)$$

$$= \frac{1 + \sqrt{1-q^2}}{2} \tag{9d}$$

The diradical character dependences of these quantities for $r_K = 0$ (the usual case) are sketched in Figure 1c. The transition moment between $|S_{1g}\rangle$ and $|S_{2g}\rangle$ vanishes because they have the same g symmetry. As increasing $y$, both DL excitation energies decrease toward 1, with a rapid decrease in the small $y$ region. Starting from $(\mu_{\mathrm{DL}\,S_{1g},S_{1u}})^2 = (\mu_{\mathrm{DL}\,S_{1u},S_{2g}})^2 = 0.5$ for $y = 0$, $(\mu_{\mathrm{DL}\,S_{1g},S_{1u}})^2$ monotonically decreases toward 0, whereas $(\mu_{\mathrm{DL}\,S_{1u},S_{2g}})^2$ increases toward 1. These variations originate from the fact that the ionic component of state $S_{1g}$ ($S_{2g}$) decreases (increases) as a function of $y$, whereas state $S_{1u}$ keeps a pure ionic nature. Note that the real rather than dimensionless excitation energies do not only depend on $y$ but also on the amplitude of $U$ and, in addition, from eq 8, $y$ increases with $U$. Therefore, when increasing $y$, $E_{S_{1u},S_{1g}}$ decreases, reaches a stationary value, and in some cases with very large $U$ it increases again in the large $y$ region.[57] In summary, the excitation energies and other spectroscopic properties are strongly related to the diradical character of the electronic ground state.

> The excitation energies and other spectroscopic properties are strongly related to the diradical character of the electronic ground state.

*Second Hyperpolarizability As a Function of Diradical Character.* Using perturbation theory, the hyperpolarizabilities are given in terms of summation-over-states (SOS) expressions, that is, in terms of the excitation energies, transition moments and dipole moment differences between states.[95,96] For the $A^{\bullet}-B^{\bullet}$ model system, this SOS expression reduces to a three-state approximation $\{|S_{1g}\rangle, |S_{1u}\rangle$ and $|S_{2g}\rangle\}$ and, in the static limit, the diagonal $\gamma_{iiii}$ component (with $i$ the direction of the bond axis, and hereafter referred to as $\gamma$) is expressed by type II ($\gamma^{\mathrm{II}}$: the first term) and type III-2 terms ($\gamma^{\mathrm{III-2}}$: the second term),[97,98]

$$\gamma = \gamma^{\mathrm{II}} + \gamma^{\mathrm{III-2}} = -4\frac{(\mu_{S_{1g},S_{1u}})^4}{(E_{S_{1u},S_{1g}})^3} + 4\frac{(\mu_{S_{1g},S_{1u}})^2(\mu_{S_{1u},S_{2g}})^2}{(E_{S_{1u},S_{1g}})^2 E_{S_{2g},S_{1g}}} \tag{10}$$

Inserting eqs 9a-9d into 10, we obtain the dimensionless second hyperpolarizability $\gamma_{\mathrm{DL}}$ as a function of $y$ and $r_K$,[53]

$$\gamma_{\mathrm{DL}} \equiv \frac{\gamma}{(R_{\mathrm{BA}}^4/U^3)}$$

$$= \frac{\gamma^{\mathrm{II}}}{(R_{\mathrm{BA}}^4/U^3)} + \frac{\gamma^{\mathrm{III-2}}}{(R_{\mathrm{BA}}^4/U^3)}$$

$$= -\frac{8(1-y)^4}{\{1 + \sqrt{1-(1-y)^2}\}^2\left\{1 - 2r_K + \frac{1}{\sqrt{1-(1-y)^2}}\right\}^3}$$

$$+ \frac{4(1-y)^2}{\left\{1 - 2r_K + \frac{1}{\sqrt{1-(1-y)^2}}\right\}^2\left\{\frac{1}{\sqrt{1-(1-y)^2}}\right\}} \tag{11}$$

The variations of $\gamma_{\mathrm{DL}}^{\mathrm{II}}$ (the first term), $\gamma_{\mathrm{DL}}^{\mathrm{III-2}}$ (the second term) and $\gamma_{\mathrm{DL}}$ are shown in Figure 2a as the function of the diradical character $y$ in the case of $r_K = 0$. It is found that $\gamma_{\mathrm{DL}}$ exhibits a bell-shape variation with a maximum value at $y \sim 0.359$, which implies that systems with intermediate diradical character exhibit larger $\gamma_{\mathrm{DL}}$ than closed-shell ($y = 0$) and pure diradical ($y = 1$) systems.[53] This enhancement of $\gamma_{\mathrm{DL}}$ in the intermediate $y$ region is dominated by the contribution of type III-2 ($\gamma_{\mathrm{DL}}^{\mathrm{III-2}}$). Furthermore, as sketched in Figure 2b for $\gamma_{\mathrm{DL}}^{\mathrm{III-2}}$ with $r_K = 0$, as $y \to 0$ the denominator $(E_{\mathrm{DL}\,S_{1u},S_{1g}})^2(E_{\mathrm{DL}\,S_{2g},S_{1g}})^2$ and the numerator $(\mu_{\mathrm{DL}\,S_{1g},S_{1u}})^2(\mu_{\mathrm{DL}\,S_{1u},S_{2g}})^2$ approach infinity and a finite value, respectively, resulting in $\gamma_{\mathrm{DL}}^{\mathrm{III-2}} \to 0$, whereas as $y \to 1$ they tend toward a small though finite value and 0, leading again to $\gamma_{\mathrm{DL}}^{\mathrm{III-2}} \to 0$. Then, as increasing $y$ from 0 to 1, the denominator decreases rapidly in the small diradical character region ($y < \sim 0.2$), whereas the numerator shows a gradual decrease, the features of which result in the enhancement of $\gamma_{\mathrm{DL}}^{\mathrm{III-2}}$ in the intermediate diradical character region: $\gamma_{\mathrm{DL}}^{\mathrm{III-2}}$ takes a maximum ($\sim 0.243$) at $y \sim 0.306$. As a result, the second hyperpolarizability ($\gamma$) exhibits a strong correlation with the diradical character $y$, referred to as "$y-\gamma$ correlation": systems having intermediate $y$ values around 0.5 exhibit larger $\gamma$ amplitudes than closed-shell ($y = 0$) and pure diradical ($y = 1$) systems of similar size.

An alternative analysis of $\gamma_{\mathrm{DL}}$ is obtained as a function of $r_J$ and $r_K$, which clarifies the relationship between $\gamma_{\mathrm{DL}}$, $y$ and the magnetic interaction $r_J$. Substituting eqs 9a−9d into eq 10, we obtain
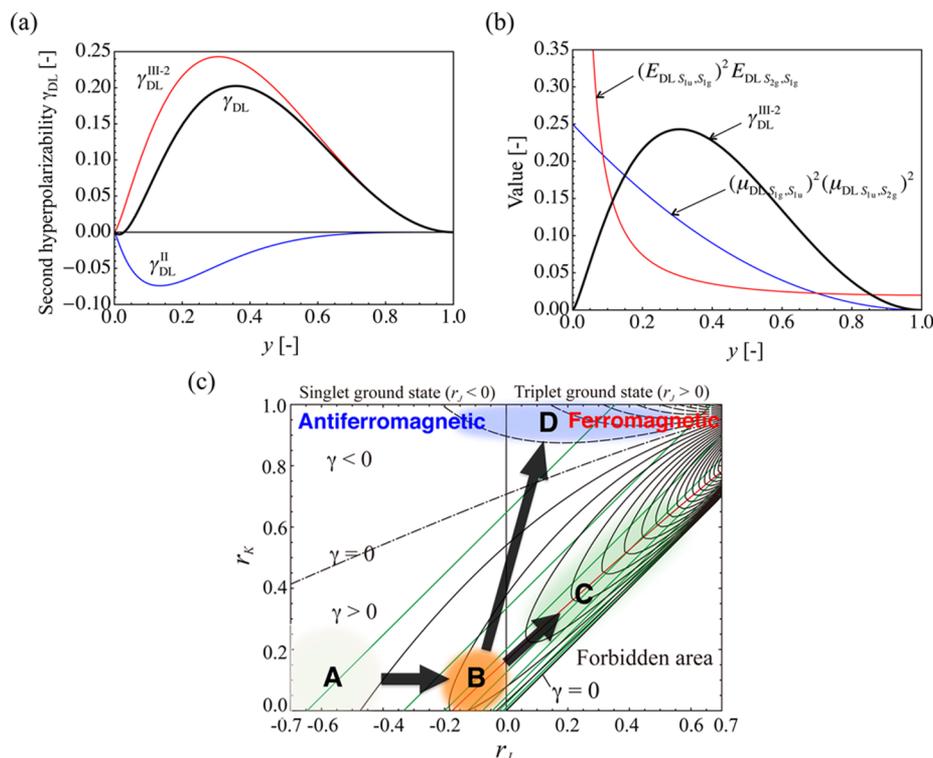
**Figure 2.** Variations of dimensionless $\gamma_{iiii}$ ($\gamma_{DL\ iiii}$), $\gamma^{II}_{iiii}$ ($\gamma^{II}_{DL\ iiii}$), and $\gamma^{III-2}_{iiii}$ ($\gamma^{III-2}_{DL\ iiii}$) as a function of diradical character ($y$) in the case of $r_K = 0$ (a), diradical character ($y$) dependences of $\gamma^{III-2}_{DL}$, $(\mu_{DL\ S_{1g}S_{1u}})^2(\mu_{DL\ S_{1u}S_{2g}})^2$ and $(E_{DL\ S_{1u}S_{1g}})^2 E_{DL\ S_{2g}S_{1g}}$ in the case of $r_K = 0$ (b), and contours of $\gamma_{DL}$ ($-2.0 \leq \gamma_{DL} < 2.0$, interval = 0.1) on the plane ($r_J$, $r_K$), where solid, dotted, and dashed black lines indicate positive, negative, and zero lines of $\gamma_{DL}$, respectively (c). In (c), the red line represents the ridge line connecting the ($r_J$, $r_K$) points giving maximum $\gamma_{DL}$ values, and the iso-$y$-lines are shown by solid green lines. Region **A** and **B**–**D** represent closed-shell (conventional NLO systems) and open-shell (theoretically predicted systems) regions, respectively, where the arrow indicates the order of exploration.

> The second hyperpolarizability ($\gamma$) exhibits a strong correlation with the diradical character $y$, referred to as "$y$–$\gamma$ correlation": systems having intermediate $y$ values around 0.5 exhibit larger $\gamma$ amplitudes than closed-shell ($y = 0$) and pure diradical ($y = 1$) systems of similar size.

$$\gamma_{DL} = \frac{\gamma}{(R^2_{BA}/U^3)}$$

$$= -\frac{4(r_K - r_J)^2}{\{1 + 2(r_K - r_J)\}^2(1 - r_J)^3}$$

$$+ \frac{4(r_K - r_J + 1)(r_K - r_J)}{\{1 + 2(r_K - r_J)\}^3(1 - r_J)^2} \tag{12}$$

The $\gamma_{DL}$ isovalue curves (black contour) are shown in Figure 2c on the ($r_J$, $r_K$) plane together with the iso-$y$-lines (green lines). The red ridge line, which connects the ($r_J$, $r_K$) points giving maximum $\gamma_{DL}$ values, is almost parallel to the iso-$y$-lines between $y = 0.3$ and 0.5. This shows that for finite $r_K$ values $\gamma_{DL}$ is enhanced in the intermediate $y$ region, similarly to the case with $r_K = 0$. As also seen from this map, the systems having open-shell singlet ground states (region **B**) exhibit larger $\gamma_{DL}$ values than the conventional closed-shell systems (region **A**), and the maximum $\gamma_{DL}$ further increases from the lower left to the upper right corner on the ($r_J$, $r_K$) plane. In particular, the systems with triplet ground states and singlet excited states with intermediate diradical characters (region **C**) are predicted to present further enhancement of $\gamma_{DL}$ (in their singlet excited state) as compared to the singlet ground-state systems with intermediate diradical characters (region **B**). Region **C** corresponds to the ferromagnetic interaction region ($J > 0$), which has been actively investigated in an effort to realize molecular magnets. Another intriguing region is region **D**, because this region, which has singlet or triplet ground states, presents negative $\gamma_{DL}$ values of large amplitudes. Although regions **C** and **D** are attractive and should be investigated in the future, we focus on the compounds belonging to region **B** in this Perspective because several real thermally stable compounds belonging to region **B** have been discovered or synthesized in recent years.[24−30]

*Asymmetric Open-Shell Singlet Systems.* Asymmetric open-shell singlet molecular systems constitute another class of compounds, where asymmetricity plays also a role on their ground- and excited-electronic structures.[90] Following the approach for symmetric systems, the $a(x)$ and $b(x)$ LNOs (eq 1) are used and defined in terms of the bonding and antibonding MOs, $g(x)$ and $u(x)$, which read

$$g(x) = \frac{1}{\sqrt{2(1 + S_{AB})}}[\chi_A(x) + \chi_B(x)]$$

$$\text{and } u(x) = \frac{1}{\sqrt{2(1 - S_{AB})}}[\chi_A(x) - \chi_B(x)] \tag{13}$$
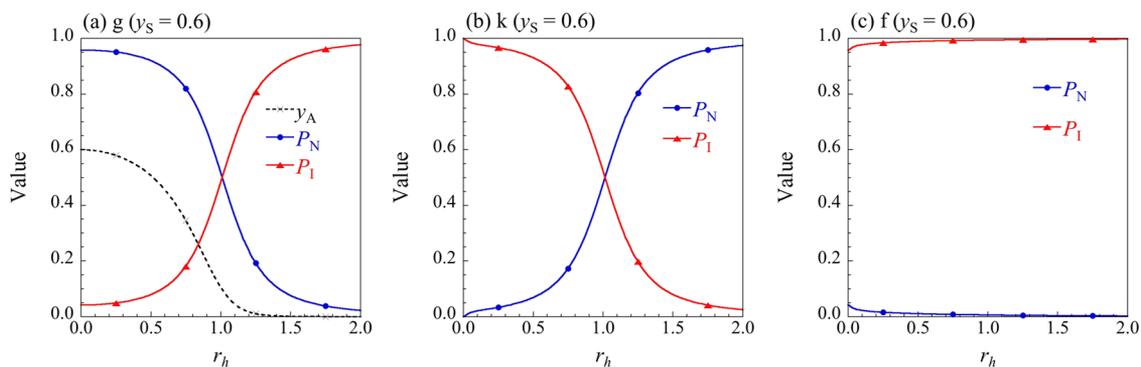
**Figure 3.** $r_h$ dependences of $P_N$ and $P_I$ in state g, k, and f for $y_S = 0.6$ (a−c). The evolution of $y_A$ (state g) as a function of $r_h$ is also displayed.

Here, the AOs are different, that is, $\chi_A(x) \neq \chi_B(x)$ and their overlap reads $S_{AB} \equiv \langle \chi_A | \chi_B \rangle$. In this case, eq 4 becomes

$$\begin{pmatrix} 0 & K_{ab} & t_{ab(aa)} & t_{ab(bb)} \\ K_{ab} & 0 & t_{ab(aa)} & t_{ab(bb)} \\ t_{ab(aa)} & t_{ab(aa)} & -h + U_a & K_{ab} \\ t_{ab(bb)} & t_{ab(bb)} & K_{ab} & h + U_b \end{pmatrix} \quad (14)$$

Here, $h$ is the one-electron core Hamiltonian difference, $h \equiv h_{bb} - h_{aa}$ set positive, where $h_{pp} \equiv \langle p | h(1) | p \rangle = \langle \overline{p} | h(1) | \overline{p} \rangle \leq 0$. Because the transfer integrals include the two-electron integral between the neutral and ionic determinants in addition to a one-electron integral (e.g., $\langle a | h(1) | b \rangle$), we obtain two types of transfer integrals, for example, $t_{ab(aa)} \equiv \langle a\overline{b} | \hat{H} | a\overline{a} \rangle$ and $t_{ab(bb)} \equiv \langle a\overline{b} | \hat{H} | b\overline{b} \rangle$, which are different because $(ab|aa) \neq (ab|bb)$. We introduce the average transfer integral, $t_{ab} \equiv (t_{ab(aa)} + t_{ab(bb)})/2$. $U_a$ and $U_b$ are defined by $U_a \equiv U_{aa} - U_{ab} + X$ and $U_b \equiv U_{bb} - U_{ab} - X$,[90] where $X \equiv \sum_c^{core} \{2(U_{ac} - U_{bc}) - (K_{ac} - K_{bc})\}$ becomes zero for symmetric molecular systems and $U_a (= U_b)$ describes the effective Coulomb repulsion, that is, the difference between the on-site $[U_{aa} (= U_{bb})]$ and intersite $(U_{ab})$ Coulomb integrals. Using the average effective Coulomb repulsion $U[\equiv (U_a + U_b)/2]$, the dimensionless quantities are defined by[90]

$$\frac{|t_{ab}|}{U} \equiv r_t (\geq 0), \quad \frac{2K_{ab}}{U} \equiv r_K (\geq 0), \quad \frac{h}{U} \equiv r_h (\geq 0), \quad \frac{U_a}{U_b}$$

$$\equiv r_U (\geq 0), \quad \text{and} \quad \left| \frac{t_{ab(aa)}}{t_{ab(bb)}} \right| \equiv r_{tab} (\geq 0) \quad (15)$$

The last three parameters determine the degree of asymmetric electron distribution, where larger population on A than on B is caused by the increase in $r_h (\geq 0)$ or by the decrease in $r_U (\leq 1)$ or by $r_{tab} (\leq 1)$. Because the LNOs $a$ and $b$ are well localized on sites A and B, the difference between $t_{ab(aa)}$ and $t_{ab(bb)}$ is assumed negligible, that is, $r_{tab} \sim 1$, as compared to the difference between $h_{aa}$ and $h_{bb}$ and that between $U_{aa}$ and $U_{bb}$. Here, we consider the change in $r_h$ between 0 and 2 with keeping $(r_U, r_{tab}) = (1, 1)$ for simplicity, which corresponds to the situation where the asymmetricity is primarily governed by the difference of ionization potentials of the constitutive atoms/sites A and B. We next introduce the pseudodiradical character $y_S$ as an alternative to $r_t$[90]

$$y_S = 1 - \frac{4r_t}{\sqrt{1 + 16r_t^2}} \quad (16)$$

which reduces to the diradical character for the symmetric system (eq 8), that is, with $(r_h, r_U, r_{tab}) = (0, 1, 1)$. The diradical character of asymmetric systems is referred to as $y_A$, which is a function of $(r_t, r_K, r_h, r_U, r_{tab})$. By solving the VCI eigenvalue equation, we obtain the eigenvalues and eigenvectors as a function of $(r_t, r_K, r_h, r_U, r_{tab})$ or of $(y_S, r_K, r_h, r_U, r_{tab})$. The eigenvalues and eigenvectors are represented by $\{j\} = \{T, g, k, f\}$ (T: triplet state, and g, k, f: singlet states) and $\{C_{a\overline{b},j}, C_{b\overline{a},j}, C_{a\overline{a},j}, C_{b\overline{b},j}\}$, respectively

$$|\Psi_j\rangle = C_{a\overline{b},j} |a\overline{b}\rangle + C_{b\overline{a},j} |b\overline{a}\rangle + C_{a\overline{a},j} |a\overline{a}\rangle + C_{b\overline{b},j} |b\overline{b}\rangle \quad (17)$$

Using the MOs (g and u) (see eq 13), we can construct an alternative basis set $\{|G\rangle = |g\overline{g}\rangle, |S\rangle = (1/2)[|g\overline{u}\rangle - |\overline{g}u\rangle], |D\rangle = |u\overline{u}\rangle\}$ for the singlet states, which represent the ground, the singly excited, and the doubly excited determinants, and obtain the eigenvalues and eigenfunctions by solving the VCI eigenvalue equation in the MO representation.[90] For example, the ground state is represented by

$$|\Psi_g\rangle = \xi |G\rangle + \eta |S\rangle - \zeta |D\rangle \quad (18)$$

which satisfies the normalization condition: $\xi^2 + \eta^2 + \zeta^2 = 1$. By comparing eq 18 with eq 17, we obtain the relations

$$\xi = C_{a\overline{b},g} + \frac{1}{2}(C_{a\overline{a},g} + C_{b\overline{b},g}), \quad \eta = \frac{1}{\sqrt{2}}(C_{a\overline{a},g} - C_{b\overline{b},g}),$$

$$\text{and} \quad \zeta = C_{a\overline{b},g} - \frac{1}{2}(C_{a\overline{a},g} + C_{b\overline{b},g}) \quad (19)$$

From the eigenfunctions, we consider the evolution of the neutral $(P_N)$ and ionic $(P_I)$ populations of the three singlet states $\{g, k, f\}$ as a function of $r_h$, where $P_N = |C_{a\overline{b},i}|^2 + |C_{b\overline{a},i}|^2$ and $P_I = |C_{a\overline{a},i}|^2 + |C_{b\overline{b},i}|^2$ for state $i$. Figure 3 shows the $r_h$ dependences of $P_N$ and $P_I$ for $r_K = 0$ and different values of $y_S$ (or $r_t$). $P_N$ and $P_I$ display mirror evolution as a function of $r_h$ (with respect to $P_N = P_I = 1/2$ because $P_N + P_I = 1$). As seen from Figure 3a, in the ground state, $P_N$ decreases ($P_I$ increases) with $r_h$, so that the $P_N$ and $P_I$ curves intersect at $r_h \sim 1$ for $y_S = 0.6$. In contrast, in the first excited state (Figure 3b), $P_I$ decreases from 1 ($P_N$ increases from 0) and, again, $P_I$ and $P_N$ intersect around $r_h = 1.0$. Namely, for intermediate $y_S$ values, the increase in $r_h$ causes the inversion of the dominant electronic configurations (neutral/ionic) in states g and k around $r_h = 1$, which supports the decrease of $y_A$ toward 0 for $r_h > 1$ as shown in Figure 3a. In state f (Figure 3c), $P_I$ slightly increases ($P_N$ slightly decreases) with $r_h$ though an almost pure ionic state is observed at any $r_h$. The $P_N = P_I$ relationship at $r_h \sim 1$ for $y_S > 0$ is qualitatively understood by the fact that $h (= h_{bb} - h_{aa}) \sim U$ corresponds to the situation where the attracting and repulsion energies between a pair of electrons in LNOs $a$ and $b$ are similar, which equalizes $P_N$ with $P_I$ in the case of small transfer integral
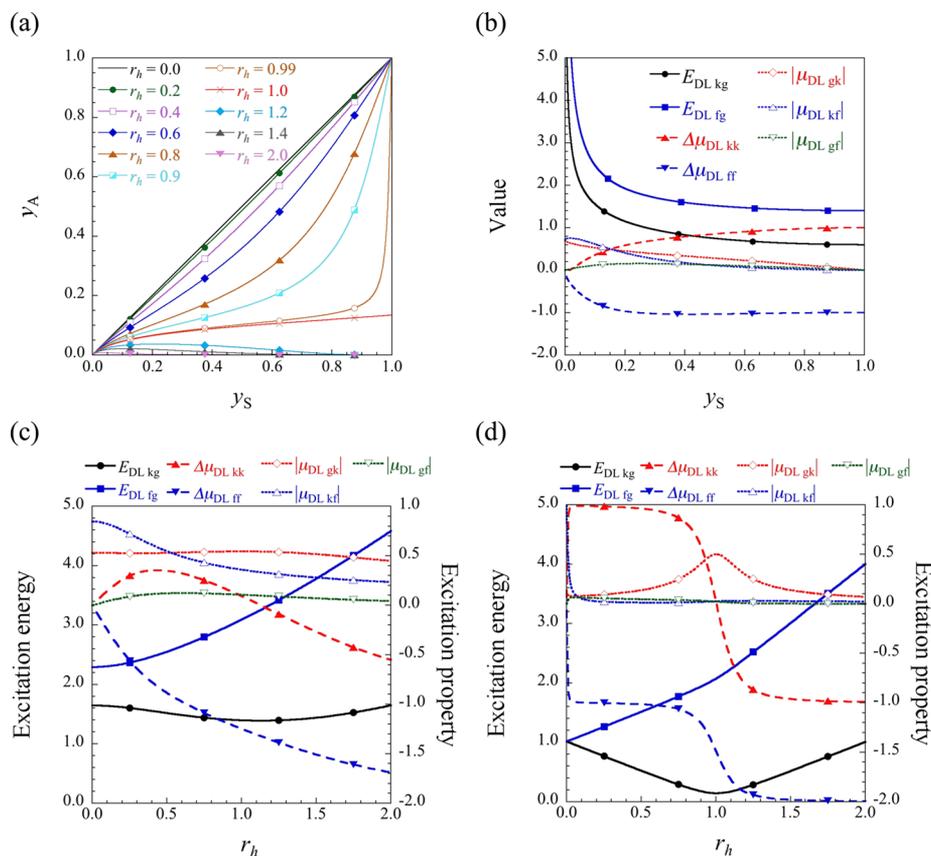
**Figure 4.** $y_S$ versus $y_A$ plots for $r_h = 0.0-2.0$ (a), and $y_S$ dependences of dimensionless excitation energies $E_{DL\,ij}$, transition moment amplitudes $|\mu_{DL\,ij}|$ and dipole moment differences $\Delta\mu_{DL\,ii}$, where $i$ = g, k, and f, for $r_h = 0.4$ (b). Asymmetricity ($r_h$) dependences of the dimensionless excitation energies and properties for different pseudodiradical characters $y_S = 0.1$ (c) and 0.8 (d).

(which is realized for $y_S > 0$). Next, we consider the asymmetricity ($r_h$) dependence of the diradical character $y_A$, as given by $n_{LUNO}$. Using eq 18, $y_A$ reads[90]

$$y_A \equiv n_{LUNO} = 1 - |\xi - \zeta|\sqrt{2 - (\xi - \zeta)^2} \qquad (20)$$

For symmetric systems, eq 20 reduces to the usual definition, twice the weight of the doubly excitation configuration[53]

$$y_A = y_S = 2\zeta^2 \qquad (21)$$

Using eqs 19 and 20, the diradical character $y_A$ can also be expressed as a function of the LNO coefficients[90]

$$y_A = 1 - |C_{a\bar{a},g} + C_{b\bar{b},g}|\sqrt{2 - (C_{a\bar{a},g} + C_{b\bar{b},g})^2} \qquad (22)$$

For asymmetric systems, this equation indicates that the ionic configuration with asymmetric distribution ($|C_{a\bar{a},g}| \neq |C_{b\bar{b},g}|$) decreases the diradical character $y_A$, for example, $y_A = 0$ for ($C_{a\bar{a},g} = 1$ and $C_{b\bar{b},g} = C_{a\bar{b},g} = C_{b\bar{a},g} = 0$). Figure 4a shows the relationship between $y_S$ (eq 16) and $y_A$ (eqs 20 and 22) for asymmetricity $r_h$ ranging between 0.0 and 2.0. $y_A$ is systematically smaller than $y_S$, in particular in the intermediate $y_S$ region when increasing $r_h$. It is also found that for $y_S = 1$, $y_A = 1$ for $r_h < 1$, but $y_A = 0$ for $r_h > 1$, whereas $y_A$ is close to ~0.134 for $r_h = 1$. This behavior originates from the exchange of dominant configuration (neutral/ionic) in state g between $r_h < 1$ and $r_h > 1$ for $y_S > 0$.

Then, the dependences of the dimensionless excitation energies [$E_{DL\,ij} \equiv (E_i - E_j)/U$], transition moment amplitudes ($|\mu_{DL\,ij}| \equiv |\mu_{ij}|/R_{BA}$) and dipole moment differences [$\Delta\mu_{DL\,ii} \equiv (\mu_{ii} - \mu_{gg})/R_{BA}$] are sketched as a function of $y_S$ for $r_h = 0.4$

(Figure 4b).[90] We here assume that $(a|r_1|b) \sim 0$, because the LNOs $a$ and $b$ are well localized on each site and the overlap between $a$ and $b$ is zero by definition. The $y_S$ dependences of these quantities for $r_h = 0$ (symmetric system) are already shown in Figure 1c, where $S_{1g} = g$, $S_{1u} = k$, and $S_{2g} = f$. When $r_h = 0.4$, upon increasing $y_S$, the amplitudes of $\Delta\mu_{DL\,kk}$ (positive) and $\Delta\mu_{DL\,ff}$ (negative) increase. These dipole moment differences indicate that the polarizations in states g and k have the same direction (from A to B), which is opposite to that in state f. Then, both $|\mu_{DL\,gk}|$ and $|\mu_{DL\,kf}|$ decrease toward zero with increasing $y_S$ in contrast to the symmetric case ($r_h = 0$) (Figure 1c). Finally, both $E_{DL\,fg}$ and $E_{DL\,kg}$ decrease with $y_S$, though they are larger and smaller than those of the symmetric case ($r_h = 0$), respectively. Indeed, $E_{DL\,fg} = 1 + r_h$ and $E_{DL\,kg} = 1 - r_h$ at $y_S = 1$.[90] As seen from Figure 3, when $r_h$ becomes larger than 1, the dominant configurations are exchanged between states g and k, which leads to the sign change of $\Delta\mu_{DL\,kk}$ at $r_h \sim 1$ ($\Delta\mu_{DL\,kk} > 0$ for $r_h < 1$ and $\Delta\mu_{DL\,kk} < 0$ for $r_h > 1$), and for $r_h > 1$, its amplitude increases with $y_S$ due to the increase of diradical (ionic) configuration in state k (g). It is also found analytically that for $y_S = 1$ and $r_h > 1$ $E_{DL\,fg} = 2r_h$ and $E_{DL\,kg} = r_h - 1$, which causes the increase in $E_{DL\,kg}$ after reaching a minimum at $r_h \sim 1$ though $E_{DL\,fg} = 2r_h$ continues to increase with $r_h$ (see Figure 4c, d). On the other hand, for $r_h \sim 1$, $E_{DL\,kg}$ reduces to 0 as increasing $y_S$, whereas $\Delta\mu_{DL\,kk}$ is close to 0 and $|\mu_{DL\,gk}|$ is almost constant (and nonzero) in the whole $y_S$ range. This reflects the equal weight of the neutral and ionic configurations in both states as shown in Figure 3. Next, we show the $r_h$ dependences of the excitation energies and excitation properties for different pseudo diradical characters $y_S = 0.1$ and
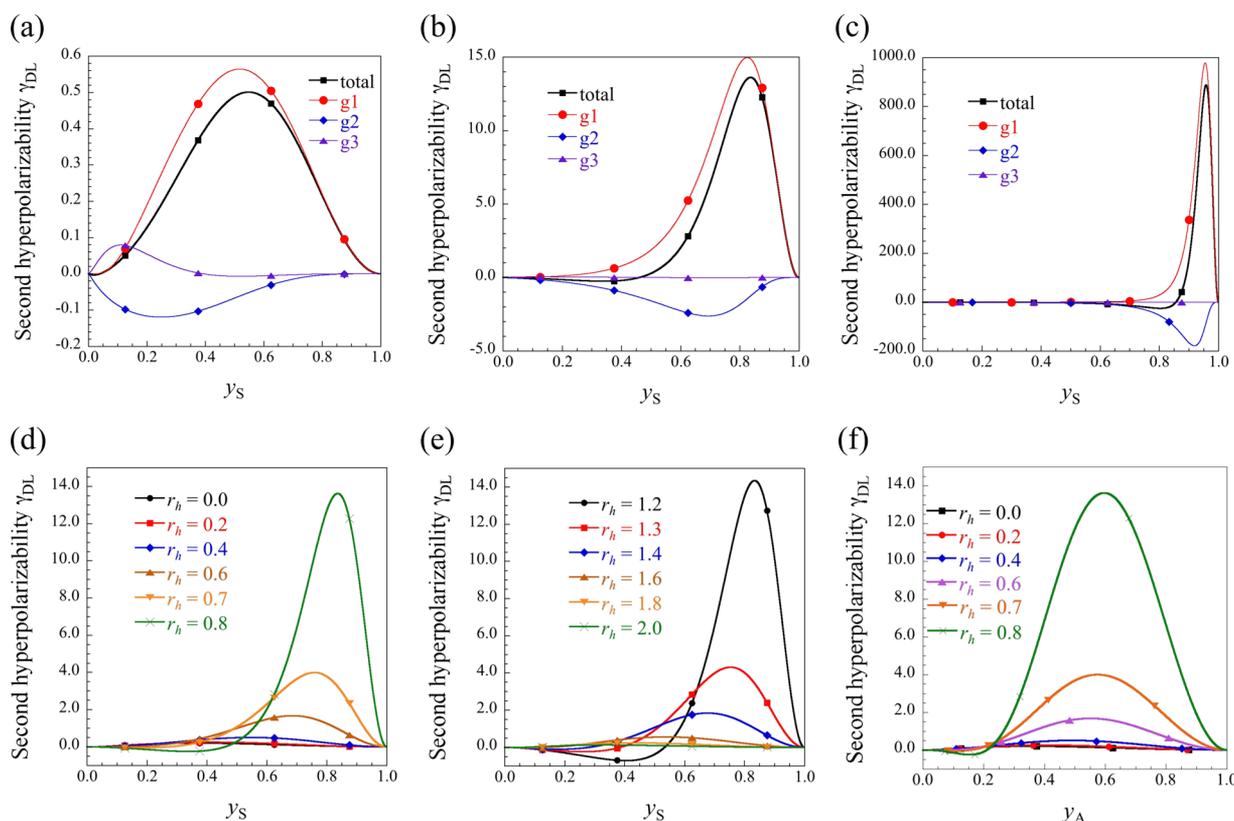
**Figure 5.** $y_S$ dependences of $\gamma_{DL}$ [total, Type I(g1), Type II(g2), and Type III(g3)] for $r_h = 0.4$ (a), 0.8 (b), and 0.95 (c). Diradical character dependences of $\gamma_{DL}$ as a function of $r_h$: $y_S - \gamma_{DL}$ for $r_h = 0.0-0.8$ (d) and 1.2-2.0 (e), as well as $y_A - \gamma_{DL}$ for $r_h = 0.0-0.9$ (f).

0.8 (Figure 4c and f). In the case of $y_S = 0.1$, $E_{DL\ kg}$ displays a weak minimum at $r_h \sim 1$, whereas $E_{DL\ fg}$ increases with $r_h$. $|\mu_{DL\ gk}|$ ($|\mu_{DL\ gf}|$) remains close to 0.5 (negligible), whereas $|\mu_{DL\ kf}|$ decreases with $r_h$. The increase followed by a decrease of $\Delta\mu_{DL\ kk}$ as a function of $r_h$, which is positive then negative for $r_h < 1$ and $r_h > 1$, respectively, reflects the exchange of the dominant ionic and neutral configurations with respect to $r_h \sim 1$ as shown in Figure 3. As increasing $y_S$, the rapid change of $\Delta\mu_{DL\ kk}$ from positive to negative value (together with a significant change in amplitude), the maximization of $|\mu_{DL\ gk}|$, and the minimization of $E_{DL\ kg}$ at $r_h \sim 1$ are intensified, the feature of which will govern the $r_h$ dependence of $\gamma$ for asymmetric diradical systems.[90]

*Asymmetricity Dependence of Hyperpolarizabilities.* Third, we clarify the $r_h$ dependence of $\gamma$ based on the above $r_h$-dependences of the excitation energies and properties. Owing to asymmetricity, with respect to eq 10, the $\gamma$ expression contains additional terms, in particular those associated with $\Delta\mu_{ii'}$.[90] $\gamma$ is now partitioned into three terms: I(g1), II(g2), and III(g3) = III-1(g31) + III-2(g32)[97,98]

$$\gamma^{I} = 4\frac{(\mu_{kg})^2(\Delta\mu_{kk})^2}{(E_{kg})^3} + 4\frac{(\mu_{fg})^2(\Delta\mu_{ff})^2}{(E_{fg})^3} \tag{23a}$$

$$\gamma^{II} = -4\frac{(\mu_{kg})^4}{(E_{kg})^3} - 4\frac{(\mu_{fg})^4}{(E_{fg})^3} - 4\frac{(\mu_{kg})^2(\mu_{fg})^2}{E_{kg}(E_{fg})^2}$$
$$- 4\frac{(\mu_{fg})^2(\mu_{kg})^2}{E_{fg}(E_{kg})^2} \tag{23b}$$

$$\gamma^{III-1} = 8\frac{\mu_{gk}\Delta\mu_{kk}\mu_{kf}\mu_{fg}}{(E_{kg})^2E_{fg}} + 8\frac{\mu_{gf}\Delta\mu_{ff}\mu_{fk}\mu_{kg}}{(E_{fg})^2E_{kg}}$$

$$\text{and } \gamma^{III-2} = 4\frac{(\mu_{gk})^2(\mu_{kf})^2}{(E_{kg})^2E_{fg}} + 4\frac{(\mu_{gf})^2(\mu_{fk})^2}{(E_{fg})^2E_{kg}} \tag{23c}$$

First, the $y_S$ dependences of $\gamma_{DL}$ [total, type I(g1), II(g2), III(g3)] are investigated for $r_h = 0.4$ (a), 0.8 (b), and 0.95 (c) (Figure 5). Similar to the symmetric case (Figure 2a), the total $\gamma_{DL}$ exhibits a bell-shape variation as a function of $y_S$. Then, upon increasing $r_h$ (<1), $\gamma_{DL\ max}$ is significantly enhanced and $y_{Smax}$ moves to higher $y_S$. $\gamma_{DL}$ is dominated by g1 (positive) for the whole $y_S$ and $r_h$ (<1) ranges, whereas g2 (negative) is shown to slightly shifts the $\gamma_{DL\ max}$ toward larger $y_S$. In particular, g1 is determined by the increase in $|\Delta\mu_{DL\ kk}|$ and the decrease in $E_{DL\ kg}$ with $r_h$ (<1) as well as by the increase in $|\mu_{DL\ gk}|$ around $r_h = 1$ with $y_S$. Furthermore, as shown in Figure 5d and e, $\gamma_{DL\ max}$ (positive) increases and $y_{Smax}$ moves to higher $y_S$ region for $r_h < 1$, whereas $\gamma_{DL\ max}$ (positive) decreases and $y_{Smax}$ moves to lower $y_S$ region for $r_h > 1$. In addition, for $r_h$ close to 1, we observe the emergence of negative $\gamma_{DL}$ in the intermediate $y_S$ region, for example, negative $\gamma_{DL\ max} = -0.250$ (−0.713) at $y_S = 0.339$ (0.404) for $r_h = 0.8$ (1.2). This is caused by the g2 term. The mirror symmetry of the $r_h$ dependences of $\gamma_{DL\ max}$ and $y_{Smax}$ for $r_h > 1$ with respect to those for $r_h < 1$ is caused by the inversion in $E_{DL\ kg}$, $\Delta\mu_{DL\ kk}$, and $|\mu_{DL\ gk}|$ with respect to $r_h \sim 1$ for intermediate and large $y_S$ (see Figure 4d). Also, as seen from the $y_A - \gamma_{DL}$ plot [Figure 5f], for $r_h < 1$, $\gamma_{DL}$ is maximized for intermediate $y_A$ values for any $r_h$, and $\gamma_{DL\ max}$ increases with $r_h$, as a result of the $y_S - y_A$ relationship (Figure 4a). Next, we examine the $r_h$ dependence of $\gamma_{DL}$ for different $y_S$ (Figure 6a). The shape of the $\gamma_{DL}$ variations as a function of $r_h$ do

(a)

(b)
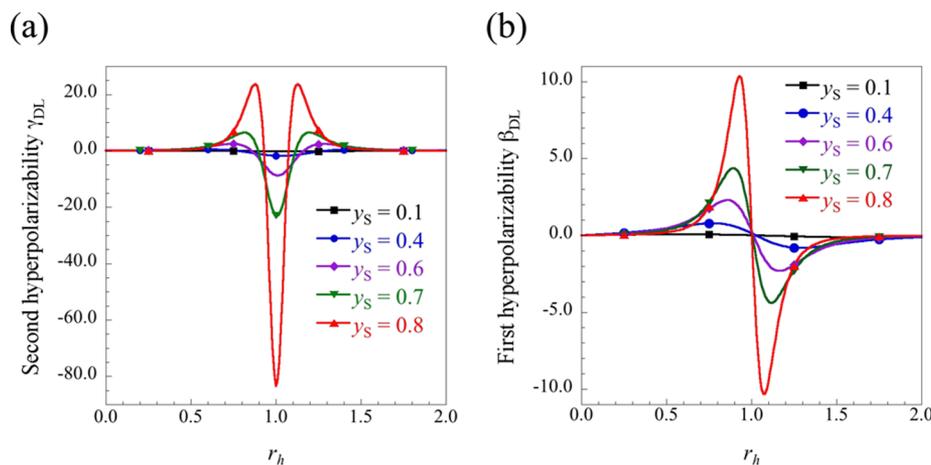


**Figure 6.** $r_h$ dependences of $\gamma_{DL}$ (a) and $\beta_{DL}$ for $y_S$ ($0.1 \leq y_S \leq 0.8$).

not depend on $y_S$, whereas their amplitudes and the $r_h$ values giving local $\gamma_{DL}$ extrema are different from each other. As increasing $r_h$, the positive $\gamma_{DL}$ increases, attains a maximum, decreases toward a negative peak value, and then increases, becomes positive again, and attains a maximum before tending to zero. Here, the amplitude of the negative peak is shown to be larger than that of the positive one. As increasing $y_S$, the amplitudes of the $\gamma_{DL}$ variations get larger and the positive peaks get closer to the negative peak ($r_h = 1$). Negative $\gamma_{DL}$ occurs when $|g1(\text{positive})| < |g2(\text{negative})|$ in eqs 23a and 23b, which corresponds to $|\Delta\mu_{DL\ kk}| < |\mu_{DL\ gk}|$ and from Figure 4d, this is satisfied by a rapid fall of $|\Delta\mu_{DL\ kk}|$ toward zero as well as by a peak growing of $|\mu_{DL\ gk}|$ around $r_h = 1$ for intermediate and large $y_S$. As a result, the introduction of asymmetric electron distribution to open-shell singlet molecular systems causes remarkable enhancements of the local maximum $\gamma_{DL}$ amplitudes as compared to corresponding closed-shell asymmetric systems. On the other hand, a slight decrease in $\gamma_{DL}$ is observed in the case of large $y_S$ in the region with large $|1 - r_h|$, and a negligible $\gamma_{DL}$ is also observed for $r_h$ close to 1, where the $\gamma_{DL}$ sign change occurs. Such large asymmetricity ($r_h$) can be realized by introducing strong donor/acceptor substituents or by applying intense static electric field. Similarly, the first hyperpolarizability $\beta_{DL}$ that exists only for asymmetric systems and that are also found to exhibit a bell-shape variation as a function of $y_S$ shows an enhanced behavior (with local positive and negative extrema of $\beta_{DL}$ in the nonzero but small $|1-r_h|$ region) as a function of $r_h$ for intermediate/large $y_S$ region with respect to the closed-shell region (see Figure 6b).[90] These results indicate that asymmetric open-shell singlet systems are promising candidates for building materials with both large second- and third-order NLO responses, which are superior to those of traditional closed-shell and symmetric intermediate open-shell singlet NLO systems. Asymmetric open-shell singlet systems are promising candidates for building materials with large second- and third-order NLO responses, which are superior to those of the corresponding asymmetric closed-shell and symmetric open-shell analogues, respectively. *Dynamic NLO Properties.* We next examine the dynamic (frequency-dependent) NLO properties because practical measurements and applications are based on dynamic properties. As an example, we investigate the two-photon absorption (TPA), which is a typical resonant third-order NLO property. The TPA

> Asymmetric open-shell singlet systems are promising candidates for building materials with large second- and third-order NLO responses, which are superior to those of the corresponding asymmetric closed-shell and symmetric open-shell analogues, respectively.

cross section of the two-site symmetric diradical system at photon energy $\hbar\omega_{ph}$ reads[93]

$$\sigma^{(2)}(\omega_{ph}) = \left( \frac{16\pi^2}{5c^2n^2\hbar} \right)(\hbar\omega_{ph})^2$$

$$\left\{ \frac{\mu^2_{S_{1g},S_{1u}}\mu^2_{S_{1u},S_{2g}}}{(E_{S_{1u},S_{1g}} - \hbar\omega_{ph})^2 + \Gamma^2_{S_{1u},S_{1g}}} \right\}$$

$$\left\{ \frac{\Gamma_{S_{2g},S_{1g}}}{(E_{S_{2g},S_{1g}} - 2\hbar\omega_{ph})^2 + \Gamma^2_{S_{2g},S_{1g}}} \right\} \quad (24)$$

where $n$ is the refractive index of the sample. The damping factor from state $\beta$ to $\alpha$, $\Gamma_{\beta\alpha}$, is assumed to satisfy the $\Gamma_{\beta\alpha} = f_{\beta\alpha}E_{\beta\alpha}$ relationship, where the coefficient $f_{\beta\alpha}$ ($0 \leq f_{\beta\alpha} \leq 1$) describes the excitation energy dependence of the damping factor, that is, the larger the excitation energy, the larger the damping factor. Therefore

$$\frac{\Gamma_{S_{1u},S_{1g}}}{\Gamma_{S_{2g},S_{1g}}} = \frac{f_{S_{1u},S_{1g}}E_{S_{1u},S_{1g}}}{f_{S_{2g},S_{1g}}E_{S_{2g},S_{1g}}} \equiv pr_E \quad (25)$$

Here $r_E$ indicates the excitation energy ratio $E_{S_{1u},S_{1g}}/E_{S_{2g},S_{1g}}$ ($0 \leq r_E \leq 1$) and $p$ is the coefficient ratio $f_{S_{1u},S_{1g}}/f_{S_{2g},S_{1g}}$ ($0 \leq p \leq 1$). Substituting eqs 9a−9d into eqs 24 and 25, the dimensionless TPA cross section satisfying $2\hbar\omega_{ph} = E_{S_{2g},S_{1g}}$ reads[93]

$$\sigma_{DL}^{(2)}(\omega_{S_{2g},S_{1g}}/2) \equiv \frac{\sigma^{(2)}(\omega_{S_{2g},S_{1g}}/2)}{\left(\frac{16\pi^2}{5c^2n^2\hbar}\right)\frac{(eR_{BA})^4}{U}} = \frac{(1-y)^2}{4f_{S_{2g},S_{1g}}\sqrt{1-(1-y)^2}\left\{(1-2r_K)^2 + p^2f_{S_{2g},S_{1g}}^2\left(1-2r_K+\frac{1}{\sqrt{1-(1-y)^2}}\right)^2\right\}} \tag{26}$$

which highlights the dependences of $\sigma_{DL}^{(2)}(\omega_{S_{2g}S_{1g}}/2)$ with respect to ($y(=y_S)$, $r_K$, $p$, $f_{S_{2g}S_{1g}}$). We here consider the dependences of $\sigma_{DL}^{(2)}(\omega_{S_{2g}S_{1g}}/2)$ with respect to $y$ and $r_K$ by setting ($p$, $f_{S_{2g}S_{1g}}$) = (1, 0.1), which qualitatively reproduces the amplitudes of experimental damping factors.[100,101] Figure 7 shows the behavior of
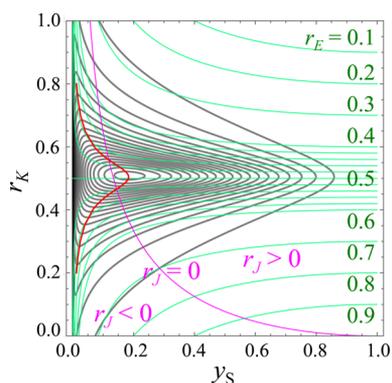


**Figure 7.** $\sigma_{DL}^{(2)}(\omega_{S_{2g}S_{1g}}/2)$ iso-contours (black lines) for ($p$,$f_{S_{2g},S_{1g}}$) = (1, 0.1) in eq 26 ($0.0 \le \sigma_{DL}^{(2)}(\omega_{S_{2g}S_{1g}}/2) \le 100.0$, interval = 5.0). The green lines indicate the iso-$r_E$ lines, the pink line is the $r_J = 0$ line, and a red line represents the ridge line connecting the ($y$, $r_K$) points exhibiting maximum $\sigma_{DL}^{(2)}(\omega_{S_{2g}S_{1g}}/2)$ at each $r_K$.

$\sigma_{DL}^{(2)}(\omega_{S_{2g}S_{1g}}/2)$ on the $y-r_K$ plane together with the isolines of excitation energy ratio $r_E$, highlighting that a one-photon resonance enhancement of the TPA peak is caused near $r_E = 0.5$ (achieved by $r_K = 0.5$) eqs 9a and 9b) in addition to the sequential TPA process. The $r_J = 0$ line (see eq 7 shows the ground-state magnetic interactions of the system: the upper and lower regions with respect to $r_J = 0$ line represent the ferromagnetic ($r_J > 0$) and antiferromagnetic ($r_J < 0$) regions,

respectively. For any $r_K$, the maximum $\sigma_{DL}^{(2)}(\omega_{S_{2g},S_{1g}}/2)$ appears in relatively small but nonzero $y$ regions, and moreover, this maximum and the corresponding $y$ value also increase when approaching $r_K = 0.5$. The iso-$\sigma_{DL}^{(2)}(\omega_{S_{2g},S_{1g}}/2)$ lines reflect the iso-$r_E$ lines, though the $\sigma_{DL}^{(2)}(\omega_{S_{2g},S_{1g}}/2)$ values approach zero values for $y \to 0$ and 1. This is understood by partitioning $\sigma_{DL}^{(2)}(\omega_{S_{2g},S_{1g}}/2)$ into the transition moment and the excitation energy contributions defined, as $(\mu_{S_{1g},S_{1u}}/eR_{BA})^2(\mu_{S_{1u},S_{2g}}/eR_{BA})^2$ and $\sigma_{DL}^{(2)}(E_{S_{2g},S_{1g}}/2)/\{(\mu_{S_{1g},S_{1u}}/eR_{BA})^2(\mu_{S_{1u},S_{2g}}/eR_{BA})^2\}$, respectively.[93] Following Figure 1c, the transition moment contribution depends only on $y$, and nonlinearly decreases from 1/4 (at $y = 0$) to 0 (at $y = 1$) with increasing $y$, whereas the excitation energy contribution provides similar isolines to $r_E$ except for the increase of the excitation energy contribution along the $r_K = 0.5$ line as a function of $y$. Again, these behaviors are related to the relative contributions of the diradical and ionic configurations in the three dominant singlet states. Because the isolines of $\sigma_{DL}^{(2)}(\omega_{S_{2g},S_{1g}}/2)$ are made by the product of these two contributions, its ($y$, $r_K$) dependence in the small and large $y$ regions is governed by the excitation energy and the transition moment contributions, respectively. In addition, the maximum $\sigma_{DL}^{(2)}(\omega_{S_{2g},S_{1g}}/2)$ value is obtained in the ground-state ferromagnetic region ($r_J > 0$) with the intermediate $y$ value around $r_K = 0.5$ ($r_E = 0.5$). As a result, the TPA resonance is enhanced for singlet diradical systems with relatively small diradical characters. On the other hand, in the ferromagnetic interaction region ($r_J > 0$), TPA is further enhanced for excited-state singlets with intermediate diradical characters. This feature is in qualitative agreement with the $y-\gamma_{DL}$ correlation (Figure 2c).[90]

A similar treatment can be applied to the dynamic third-harmonic generation (THG) hyperpolarizabilities, $\gamma(-3\omega; \omega, \omega, \omega)$. Like for the static counterpart, it has been found that the real and imaginary THG $\gamma$ peaks of symmetric systems are enhanced
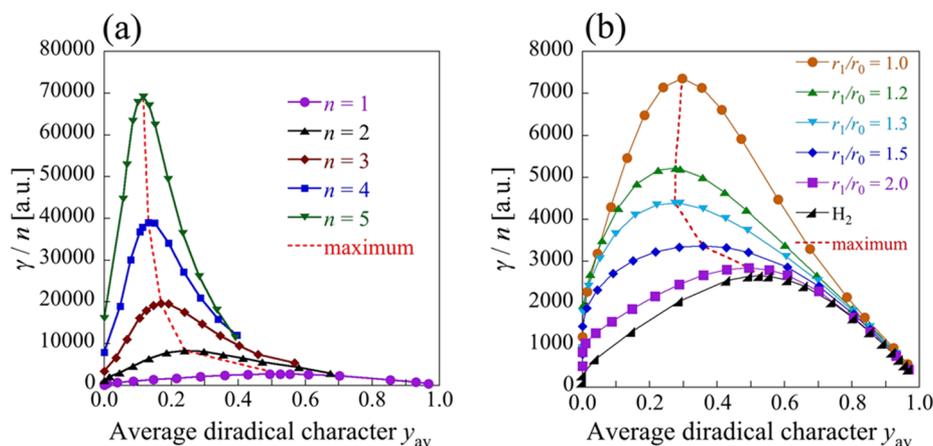


**Figure 8.** Dependence of $\gamma/n$ [a.u.] as a function of $y_{av}$. (a) The case of regular $H_{2n}$ chains ($n = 1-5$), calculated by the UCCSD(T)/(6)-31(+)+G(*)* method. (b) Alternating $H_4$ chains with $r_1/r_0 = 1.0$ (regular), 1.2, 1.3, 1.5, and 2.0, calculated by the full-CI/(6)-31(+)+G(*)* method. In (a) and (b), the dotted line represents the displacement of the maximum $\gamma/n$ value.

in the intermediate diradical character region with respect to those of closed-shell and pure diradical systems.[102] Relative positions and intensities for the two- and three-photon resonance peaks also change depending on the diradical character. In conclusion, the "$y$–$\gamma$ correlation" stating that the NLO properties are larger for intermediate diradical character compounds than for closed-shell and pure diradical compounds is valid for both static and dynamic NLO properties as well as for both symmetric and asymmetric systems.

*Multiradical NLO Systems.* Besides the attractive NLO properties of radicals at the single molecular level clarified in the above paragraphs, their supra-/supermolecular assemblies are expected to exhibit intriguing inter/intramolecular interaction effects on the multiradical character [$y_i$, determined by the occupation number of the LUNO + $i$ ($i$ = 0, 1, ...)][31,50] and then on $\gamma$. Indeed, numerous studies have already analyzed the remarkable size dependence of the NLO properties in closed-shell linear chain systems, for example, $\pi$-conjugated systems[1,16,103−108] and model hydrogen chains.[109,110] Here, we calculate the longitudinal $\gamma$ values of open-shell singlet one-dimensional (linear-chain) $H_{2n}$ ($n$ = 1−5) systems using the ab initio MO full-CI and UCCSD(T) methods.[84] These systems are regarded as models of open-shell singlet $\pi$-conjugated linear chains or of molecular aggregates composed of singlet diradical monomers. We focus on the elucidation of the relationship between the bond length (intersite distance), the bond length alternations (BLA), the average diradical character, and the longitudinal $\gamma$ value. We consider nonalternating (regular) $H_{2n}$ chains (with a unique bond distance $r_0$ and $n$ = 1, ..., 5) (b) and various alternating $H_{2n}$ chains (with two values of bond lengths, $r_0$ and $r_1$, and $r_1/r_0$ = 1.2, 1.3, 1.5 and 2.0) (c). When $r_0$ is varied from 1.0 to 4.0 Å, the diradical character ($y$) of $H_2$ goes from 0.0 (closed-shell) to 0.968 (nearly pure diradical). The variation in $\gamma/n$ for regular $H_{2n}$ chains ($r_0$ = 1.0 Å) as a function of the average diradical character $y_{av}$ is sketched in Figure 8a. At the UCCSD(T) level of approximation, the maximum $\gamma/n$ increases with chain length, whereas the average diradical character giving the maximum $\gamma/n$ value ($y_{av\ max}$) decreases. These results indicate that regular multiradical linear chains with small $y_{av}$ exhibit not only larger $\gamma/n$ amplitudes than the closed-shell analogs for small chain length but also significant chain-length dependence, demonstrating the advantage of multiradical linear chains. Figure 8b shows for $H_4$ that the BLA reduces the magnitude of $\gamma/n$ and slightly increases $y_{av\ max}$. From the chain-length dependence of $\gamma/n$ for regular $H_{2n}$ chains, we predict that singlet $\pi$-conjugated multiradical chains (aggregates) with small $y_{av}$ have the possibility of exhibiting remarkable chain-length dependence together with significant enhancements of $\gamma/n$ in comparison to conventional closed-shell $\pi$-conjugated chains of similar chain lengths.

*Design of Open-Shell Singlet NLO Systems.* In order to design open-shell NLO compounds on the basis of the $y$–$\gamma$ correlation, we need to elucidate the relationship between the diradical character and the chemical structure, for example, molecular geometry, molecular size, atomic composition, and various chemical and physical modifications. An efficient way to clarify such relationships is to invoke traditional chemical concepts and indices, for example, resonance structure, aromaticity, $\pi$-conjugation, electronegativity, donor/acceptor strength, and hybridization. Because the diradical character is a ground state property and is closely related to the effective bond strength between two unpaired electrons (see eqs 9a−9d and 11), localized on atom sites or delocalized on plural atoms, chemists are familiar with this quantity and can tune it with the aid of the

above traditional chemical concepts and indices. Here, we provide several chemical guidelines for tuning the diradical characters by presenting results on open-shell singlet molecular systems, having an intermediate diradical character. The simplest and prototype of these systems is the $H_2$ molecule under dissociation,[56,57] which exhibits a wide range of diradical character ($y$) upon $\sigma$-bond stretching and shows a maximum $\gamma$ value (along the bond axis) for intermediate $y$ value. Full-CI calculations of its excitation energies and properties have provided results in qualitative consistency with the two-site diradical model.[32,53]

Then, model and real $\pi$-bond diradicaloid systems were investigated, including *p*-quinodimethane (Figure 9),[55] twisted
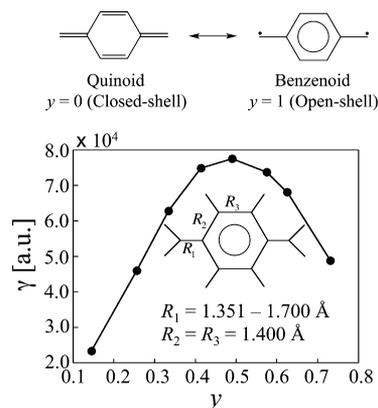


**Figure 9.** Resonance structures [quinoid (closed-shell) and benzenoid (open-shell)] of *p*-quinodimethane model and the diradical character ($y$) dependence of its $\gamma$ as evaluated at the UCCSD(T) level of approximation.

ethylene,[55] $\pi$-conjugated molecules involving imidazole (**1**) and triazole (**2**) rings,[58] diphenalenyl diradical molecules (**3, 5-9, 10, 11**),[59,60] zethrenes (**13**),[111] fullerenes (**15, 16**),[112,113] and so on (Figure 10). Table 1 lists the diradical characters and $\gamma_{zzzz}$ values for these open-shell compounds as well as for the corresponding closed-shell analogues (**2, 4, 12, 14, 17**). From these results, guidelines for realizing diradicaloids were deduced as follows (i) for condensed-ring systems having both benzenoid and quinoid resonance structures in the ground state, increasing the benzenoid (quinoid) contribution increases the diradical (closed-shell) character (Figure 9), whereas (ii) for systems involving a $\pi$-conjugated chain linking two radical moieties, decreasing the orbital interaction between the linked positions increases the diradical character. The relative benzenoid/quinoid character can be controlled by tuning the molecular architecture, including the edges form, the molecular size, the asymmetricity (for example, by introducing donor/acceptor substitutions). For instance, compound **1** involving imidazole rings has such a benzenoid/quinoid character, whereas **2** involving triazole rings only benzenoid structure. This leads to the intermediate $y$ value for **1** in contrast to **2** (nearly closed-shell), resulting in a one-order enhancement of $\gamma_{zzzz}$ for **1** as compared to **2**. For diphenalenyl diradicaloids **3**($n$), the increase of the aromaticity of the central fused-ring linker leads to the increase of the diradical character. Note here that the monotonic increase of $\gamma_{zzzz}$ with the size of **3** is simply related to the system size ($\gamma \propto R_{BA}^4$) in addition to the $y$ dependence of $\gamma_{DL}$ (see eq 11). According to the $y$–$\gamma$ correlation, $\gamma$ of IDPL [**3**(1)] with an intermediate $y$ value is enhanced by about 1 order of magnitude as compared to the closed-shell (**4**) and pure open-shell [*as*-IDPL (**5**)] analogues.[60]
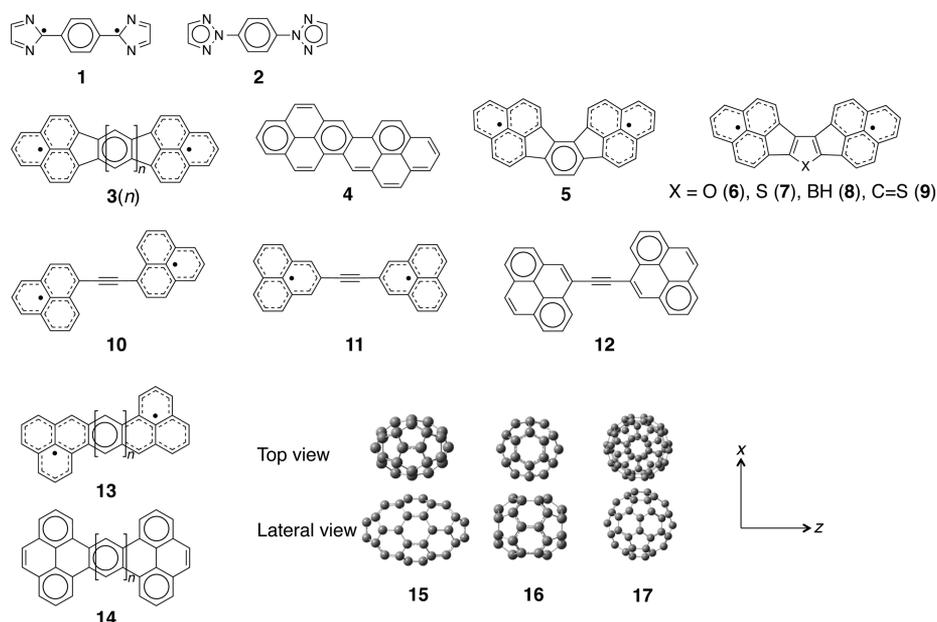
**Figure 10.** Examples of open-shell singlet molecules including bisimidazole-substituted benzene (**1**), diphenalenyl compounds (**3**(n), **5**, **6**−**8**, **10**, **11**), zethrenes (**13**(n)), and fullerenes (**15**, **16**), as well as their closed-shell analogs (**2**, **4**, **12**, **14**, **17**). Cartesian axes are also shown.

**Table 1. Diradical Characters and $\gamma_{zzzz}$ Values Calculated for Molecular Systems 1 - 37 in the Singlet States**

| compound | $y_0, y_1$ | $\gamma_{zzzz}$ [× $10^3$ a.u.] | references | compound | $y_0, y_1$ | $\gamma_{zzzz}$ [× $10^3$ a.u.] | references |
|---|---|---|---|---|---|---|---|
| 1 | $0.423^a$ | $6.53^b$ | 58 | 24(1) | $0.0^g$ | $122^g$ | 69 |
| 2 | $0.010^a$ | $0.654^b$ | 58 | 24(2) | $0.0^g$ | $492^g$ | 69 |
| 3(1) | $0.770^c$ | $2284^d$ | 59, 114 | 24(3) | $0.0^g$ | $1281^g$ | 69 |
| 3(2) | $0.854^c$ | $3342^d$ | 114 | 24(4) | $0.0^g$ | $2492^g$ | 69 |
| 3(3) | $0.901^c$ | $5143^d$ | 114 | 25(R = 2.8 Å)$^h$ | 0.776 | 1.57 | 67 |
| 4 | $0.0^a$ | $194^d$ | 59 | 26(4)$^i$ | 0.708 | 57.9 | 89 |
| 5 | $0.923^a$ | $472^d$ | 60 | 26(6)$^i$ | 0.690 | 349 | 89 |
| 6 | $0.731^c$ | $1934^d$ | 60 | 26(8)$^i$ | 0.686 | 1330 | 89 |
| 7 | $0.768^c$ | $1349^d$ | 60 | 27 | $0.975^j$ | $2.2^k$ | 72 |
| 8 | $0.374^c$ | $415^d$ | 60 | 28(Si, N) | $0.468^j$ | $57^k$ | 72 |
| 9 | $0.0^c$ | $98^d$ | 60 | 29(B, P) | $0.192^j$ | $6.6^k$ | 72 |
| 10 | $0.653^e$ | $1568^d$ | 61 | 30 | $0.684^l$ | $185^m$ | 122 |
| 11 | $0.999^e$ | $209^d$ | 61 | 31 | $0.748^l$ | $175^m$ | 122 |
| 12 | $0.192^e$ | $360^d$ | 61 | 32 | $0.143^l$ | $24.8^m$ | 55, 121 |
| 13(0) | $0.407^c$ | $375^d$ | 111 | 33 | $0.419,^f 0.041^f$ | $1140^f$ | 113 |
| 13(1) | $0.537^c$ | $863^d$ | 111 | 34 | $0.451,^f 0.047^f$ | $1307^f$ | 113 |
| 13(2) | $0.628^c$ | $1442^d$ | 111 | 35(1) | $0.485^n$ | $179^n$ | 88 |
| 14(0) | $0.0^c$ | $41^d$ | 111 | 35(2) | $0.657,^n 0.294^n$ | $1310^n$ | 88 |
| 14(1) | $0.0^c$ | $116^d$ | 111 | 35(2)$^{2+}$ | $0.597,^n 0.012^n$ | 17 300$^n$ | 88 |
| 14(2) | $0.061^c$ | $307^d$ | 111 | 36(1) | $0.0^n$ | $10.1^n$ | 88 |
| 15 | $0.701,^f 0.154^f$ | $31.4^f$ | 112 | 37 | $0.629^f$ | 83 730$^f$ | 124 |
| 16 | $0.923,^f 0.110^f$ | $3.92^f$ | 112 | | | | |
| 17 | $0.0^f$ | $3.70^f$ | 112 | | | | |
| 18 | $0.510^c$ | $145^d$ | 62 | | | | |
| 19 | $0.418^c$ | $452^d$ | 64 | | | | |
| 20 | $0.970^c$ | $199^d$ | 64 | | | | |
| 21 | $0.410,^c 0.410^c$ | $1390^d$ | 63 | | | | |
| 22 | $0.0^c$ | $417^d$ | 63 | | | | |
| 23(1) | $0.0^g$ | $17.2^g$ | 69 | | | | |
| 23(2) | $0.179^g$ | $468^g$ | 69 | | | | |
| 23(3) | $0.413^g$ | $2841^g$ | 69 | | | | |
| 23(4) | $0.776^g$ | $9800^g$ | 69 | | | | |

$^a$Calculated using PUHF/6-31G*+p. $^b$Calculated using UBHHLYP/6-31G*+p. $^c$Calculated using PUHF/6-31G*. $^d$Calculated using UBHHLYP/6-31G*. $^e$Calculated using PUHF/6-31G**. $^f$Calculated using LC-UBLYP/6-31G*. $^g$Calculated using LC-UBLYP/6-31G*+p. $^h$y(dσ) (PUHF/SDD) and γ values (UCCSD/SDD) at the bond length giving maximum γ. $^i$Average y(dσ) (PUHF/SDD) and γ values (LC-UBLYP/SDD) at the bond length of 2.8 Å. $^j$Calculated using LC-UBLYP/6-311++G**. $^k$Calculated using UCCSD(T)/6-311++G**. $^l$Calculated using PUHF/6-311+G**+LANL2DZ(d,p). $^m$Calculated using UCCSD(T)/6-311+G**+ LANL2DZ(d,p). $^n$Calculated using LC-UBLYP/6-31+G*.

The heterosubstitution of the central ring also modifies aromaticity and leads to a slight [**6** (X = O) and **7** (X = S)] or to a significant [**8** (X = BH) and **9** (X = CS)] decrease of $y$.[60] Similar relationship between the benzenoid/quinoid resonance

structures in the middle benzene rings and the diradical characters is also found in zethrenes **13**, where $y$ and $\gamma$ increase with the size so as to attain a $\gamma$ value that is 1 order of magnitude larger than in the corresponding closed-shell analogues **14**. Acetylene-linked diphenalenyl (**10**, **11**) and pyrene (**12**) compounds have intermediate diradical, pure diradical, and nearly closed-shell natures, respectively, which originates from the lack of orbital interactions at the acetylene-linked position in **11** in contrast to **10** and **12**. Accordingly, the $\gamma$ value of **10** is several-fold larger than those of **11** and **12**. For fullerenes $C_{48}$ (**15**), $C_{36}$ (**16**) and $C_{60}$ (**17**), the differences in geometry and topology significantly affect the diradical character, where the emergence of diradical character in **15** ($y = 0.701$) and **16** ($y = 0.923$) is related to the bent $sp^2$-hybridized carbon atoms for significant structural strains at the pentagon/hexagon fusion points.[112] As a result, the $\gamma$ value for **15** (intermediate diradical) is about one order larger than those of **16** (nearly pure diradical) and **17** (closed-shell).

*Polycyclic Aromatic Hydrocarbons.* The interplay between diradical character and the relative contribution of quinoid and benzenoid resonance structures is also observed in polycyclic aromatic hydrocarbons (PAHs), for example, oligoacenes and periacenes (zigzag-edged graphene nanoflakes)[30] (Figure 11).

(a)

(b)                    (c)

**18**                 **19**              **20**

(d)

**21**

(e)

**22**
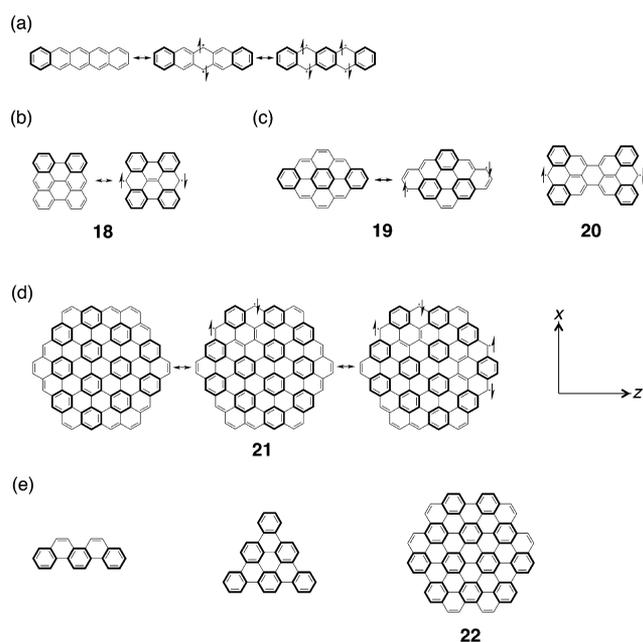
**Figure 11.** Clar's sextets in the resonance structures of (a) polycyclic aromatic hydrocarbons, oligoacenes; (b) rectangular graphene nanoflake (GNF) (PAH[3,3]) (**18**); (c) rhombic (**19**) and bow-tie (**20**) GNFs; (d) hexagonal GNF (**21**); and (e) several PAHs including only armchair edges like armchair-edged hexagonal GNF (**22**). Cartesian axes are also shown.

Their relative contributions are qualitatively predicted by the Clar's sextet rule,[115] stating that the dominant resonance structure has the most disjoint aromatic $\pi$-sextets, that is, benzene-like moieties. Indeed, for these molecules, the di-(multi)radical resonance structures are stabilized by the recovery of the aromaticity of the $\pi$-sextets, so that the contribution of di(multi)radical forms increases in the ground state. This guideline aiming at increasing $y$ is naturally associated with the molecular architectures and sizes. For example, oligoacenes display an increase of di(multi)radical characters with the size,

which increases the number of $\pi$-sextets as well as radical sites in the middle region (Figure 11a). Changing the edge shape and architectures in these PAHs significantly modifies the open-shell singlet characters (Figure 11). For example, in GNFs having only armchair edges, the closed-shell resonance forms show maximal numbers of Clar's sextets regardless of their molecular architectures including linear, trigonal, and hexagonal forms (Figure 11e). On the other hand, GNFs having zigzag edges tend to possess open-shell singlet ground states, where primary odd electron density is distributed on both-end zigzag edges (Figure 11b). In order to clarify the relationships between edge shape, $y$ and $\gamma$ values, we have calculated $\gamma_{zzzz}$ and $\gamma_{xxxx}$ (diagonal components along its zigzag and armchair edges, respectively) of PAH[3,3] (**18**) at the UBHandHLYP/6-31G* level, in its singlet and triplet states. As expected (Figure 11b), **18** has an intermediate diradical character ($y_0 = 0.510$), which is associated with odd electron densities on the mutually facing zigzag edges (Figure 12). This odd electron distribution leads to a significant

Odd electron density

$y_0 = 0.510$

$\gamma$ density

$\gamma_{xxxx} = 34.1 \times 10^3$ a.u.          $\gamma_{zzzz} = 145 \times 10^3$ a.u.
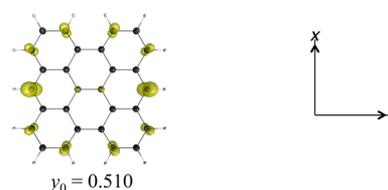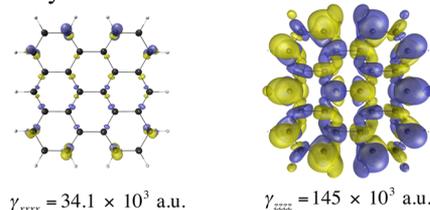
**Figure 12.** Odd electron and $\gamma$ ($\gamma_{xxxx}$ and $\gamma_{zzzz}$) density distributions of PAH[3,3] (**18**) at the UBHandHLYP/6-31G* level. $y_0$ (PUHF/6-31G*) and $\gamma$ values are given together with Cartesian axes. Yellow and blue meshes indicate positive and negative densities, respectively.

difference between $\gamma_{xxxx}$ ($34.1 \times 10^3$ a.u.) and $\gamma_{zzzz}$ ($145 \times 10^3$ au) because the intermediate diradical character is associated with the $z$ axis. Namely, the $\gamma$ is enhanced for the direction joining the radical sites. The calculations also evidenced a significant reduction of $\gamma_{zzzz}$ by going from the singlet ($\gamma_{zzzz} = 145 \times 10^3$ au) to the triplet ($\gamma_{zzzz} = 35.0 \times 10^3$ a.u.) state due to the Pauli effect in the latter[116] but a negligible difference in $\gamma_{xxxx}$. Such edge shape effects are also observed in hexagonal GNFs of similar size (**21** and **22**): the zigzag-edged form **21** presents intermediate tetraradical characters ($y_0 = y_1 = 0.410$) in contrast to its armchair-edged analogue **22** (closed-shell), and thus the $\gamma_{zzzz} = \gamma_{xxxx}$ values of **21** are more than three times as large as those of **22**. Next, we consider the architecture effects on the $y$ and $\gamma$ values by using an example of rhombic and bow-tie GNFs (Figure 11c). Consistent with the Clar's sextet rule, rhombic (**19**) and bow-tie (**20**) GNFs exhibit intermediate ($y_0 = 0.418$) and nearly pure ($y_0 = 0.970$) diradical characters, respectively, as determined at the PUHF/6-31G* level of approximation. This explains the larger $\gamma_{zzzz}$ value for the rhombic ($452 \times 10^3$ a.u.) than for the bow-tie ($199 \times 10^3$ a.u.) GNFs, as evaluated at the UBHandHLYP/6-31G* level of approximation. The odd electron density topology (related to the artifactual spin polarization of the singlet ground

(a)



(b)
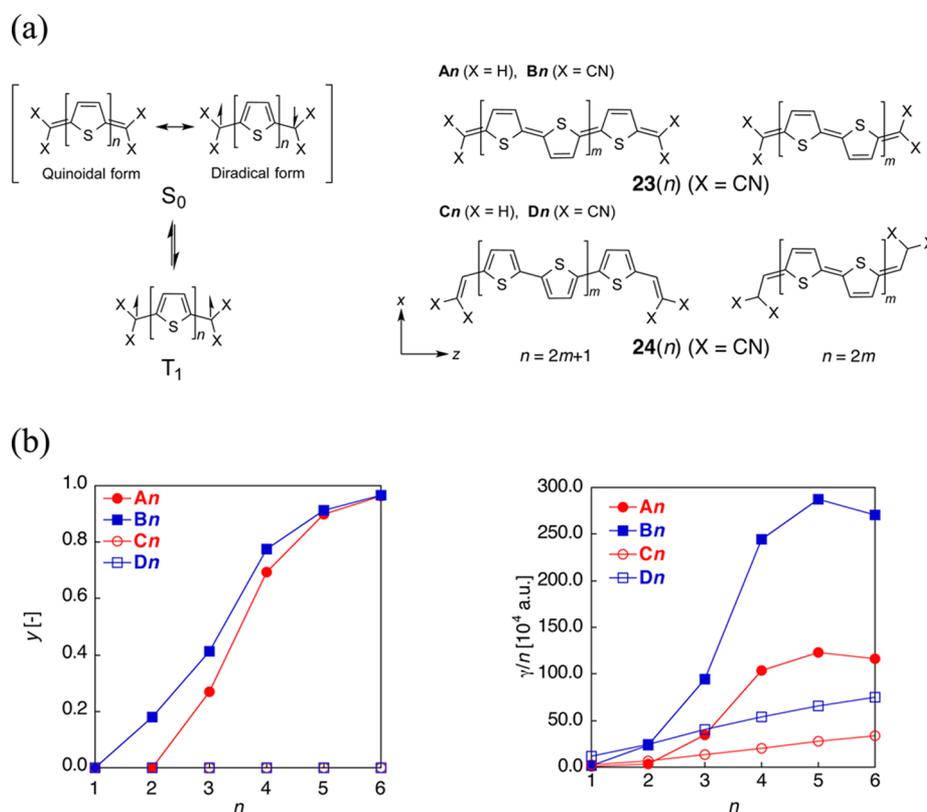


**Figure 13.** Molecular structures of singlet (S0) and triplet (T1) ground states of quinoidal oligothiophenes (QTs), and calculated models: open-shell systems **A***n* (X = H) and **B***n* (X = CN) (**23**(*n*)) and closed-shell systems **C***n* (X = H) and **D***n* (X = CN) (**24**(*n*)) for *n* = 1−6 (a). Cartesian axes are also shown. Chain-length (*n*) dependences of diradical characters (*y*) and $\gamma/n$ for the **A***n*, **B***n*, **C***n*, and **D***n* systems (b).

state in broken symmetry treatments) can also be changed by introducing 5-membered rings at the extremities of polyacenes to obtain dicyclopenta-fused acenes.[117] These substitutions have an impact on the magnetic properties (iso-chemical shieldings and magnetically induced currents), which contributes to explaining the variations on *y* and *γ*. Another example is given by the introduction of acceptor substituents at both ends of quinoidal oligothiophenes, which increase the diradical character by localizing the radicals on the terminal carbon atoms and decrease the contribution of quinoidal form (Figure 13a). Tuning the number of thiophene rings and changing the substituents at the both ends also significantly changes the diradical character and, therefore, the longitudinal *γ* amplitudes (Figure 13 and Table 1). Thus the position along the *y*−*γ* correlation curve as well as the *γ* amplitude can be tuned by carefully selecting the shape of molecular systems, in addition to their size, the presence of substituents, and so on, because it impacts the diradical character.

> The position along the *y*−*γ* correlation curve as well as the *γ* amplitude can be tuned by carefully selecting the shape of molecular systems, in addition to their size, the presence of substituents, and so on, because it impacts the diradical character.

*Transition Metal−Metal Bonded Systems.* Next, we consider systems involving transition metals, in particular, metal−metal bonded systems[67,68] because d−d orbital interactions often lead to multiple bonds of dσ, dπ, and dδ characters. These multiple bonds exhibit a whole range of diradical characters, as in the naked dichromium(II) model system.[67] Also, the effective bond orders (EBO) of such systems are generally smaller than their formal bond orders; for example, the $[Cr_2(O_2CCH_3)_4]$ dichromium(II) complex has a formal bond order of 4 but its effective bond order (EBO) is 1.99.[118] These results indicate characteristic weak metal−metal bonds and the possible emergence of singlet multiradical character. From the analysis of *γ* values of the singlet dichromium(II) $[Cr(II)−Cr(II)]$ and dimolybdenum(II) $[Mo(II)−Mo(II)]$ model systems, it was found that $\gamma(d\sigma)$ is dominant and takes a maximum value $[\gamma_{max}(d\sigma)]$ in the intermediate diradical character region of the dσ orbitals, which indicates that open-shell singlet metal−metal bonded systems belong to a novel class of "σ-dominant" third-order NLO systems [Figure 14 and Table 1 for Cr(II)−Cr(II) (**25**)]. Note from eq 11 that *γ* is also proportional to the fourth power of the distance between the radical sites and therefore that large $\gamma_{max}$ values require both intermediate diradical character and large bond lengths. Because diffuse atomic orbitals can interact with each other at long distance, which leads to an intermediate diradical character with large bond length, metal−metal bonded systems with a diffuse valence d atomic orbital are expected to satisfy the condition for enhancing $\gamma_{max}$. It was then found that smaller group number (less nuclear charge), larger period number, and smaller positive charge of transition metals generally lead to larger size of the valence d atomic orbitals and, therefore, to an intermediate dσ diradical character along with a
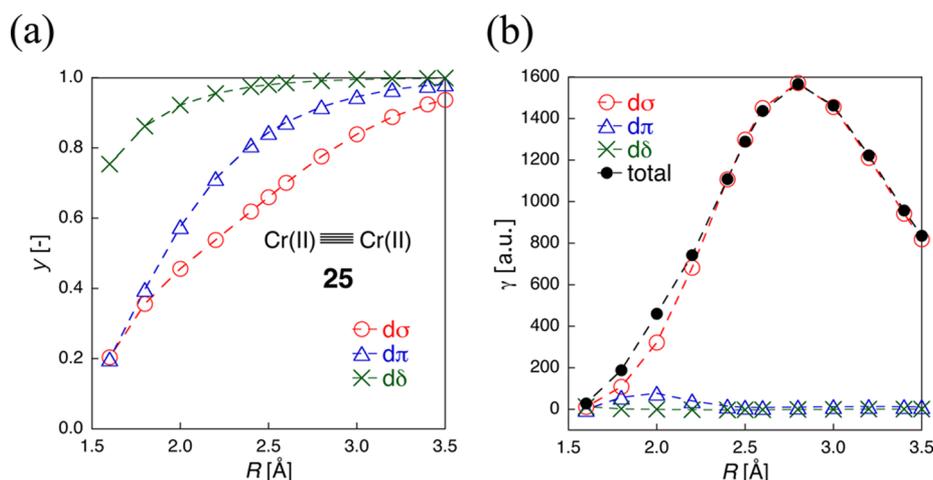
**Figure 14.** Effects of the bond length ($R$) on the UHF diradical character ($y$) (a) and on the UCCSD longitudinal second hyperpolarizability ($\gamma$) (total) (b) of Cr(II)−Cr(II) (**25**) as well as on their $d\sigma$, $d\pi$, and $d\delta$ orbital contributions.

larger bond length and a larger $\gamma_{max}$.[68] The optimal bond lengths for enhancing $\gamma$ in these dimetallic complexes, for example, 2.8 Å for Cr(II)−Cr(II) is close to the bond length (2.69 Å) of real Cr(II)−Cr(II) complexes synthesized so far.[37] Similar structure−property relationships are also observed in extended metal atomic chains (EMACs), which belong to a class of multiradical systems (see for example, Cr(II) chain **26**($n$) ($n$: the number of Cr(II) atoms, $R$ (bond length) = 2.8 Å) results in Table 1).[89] The equatorial and axial ligand effects on the open-shell character and $\gamma$ values have also been investigated, showing that the fundamental relationship between $d\sigma$ interactions and $\gamma$ is preserved and that the ligands can be used for tuning the diradical character and the bond length, and then for further enhancing $\gamma_{max}$.[119,120] These results provide a guideline for an effective molecular design of highly efficient third-order NLO systems based on metal−metal bonded systems.

*Main Group Compounds.* Among other candidates, we can consider molecules involving main group elements,[24] which are known to form relatively weak bonds originating in the weak hybridization of heavy main group elements. Recent developments toward the synthesis of thermally stable molecular systems involving such main group elements are expected to open a way to realize novel structure−NLO property relationships and to provide switching/controlling strategies of such properties. For example, using the LC-UBLYP method, one of us has investigated the open-shell characters and the $\gamma$ values of four-membered-ring diradical compounds, that is, cyclobutane-1,3-diyl (**27**), Niecke-type diradicals (**28**), and Bertrand-type diradicals (**29**) (Figure 15 and Table 1). It has been found that (i) $\gamma$ is enhanced in the intermediate $y$ region for four-membered-ring diradicals, (ii) Niecke-type diradicals with intermediate $y$ values, obtained by tuning the $E_1$ and $E_2$ combination, exhibit larger $\gamma$ values than Bertrand-type diradicals, and (iii) the $y$ value and thus $\gamma$ value can be controlled by modifying the donor/acceptor substituents attached to carbon atoms of Niecke-type $C_2P_2$ diradicals. These results demonstrate that four-membered-ring diradicals with heavy main group elements exhibit high controllability of the diradical character and thus of $\gamma$, the feature of which indicates potential applications of four-membered-ring diradicals as a building block of highly efficient open-shell NLO materials.

*Intramolecular Charge Transfer Effects in Open-Shell Singlet Systems.* The design guidelines for achieving large NLO
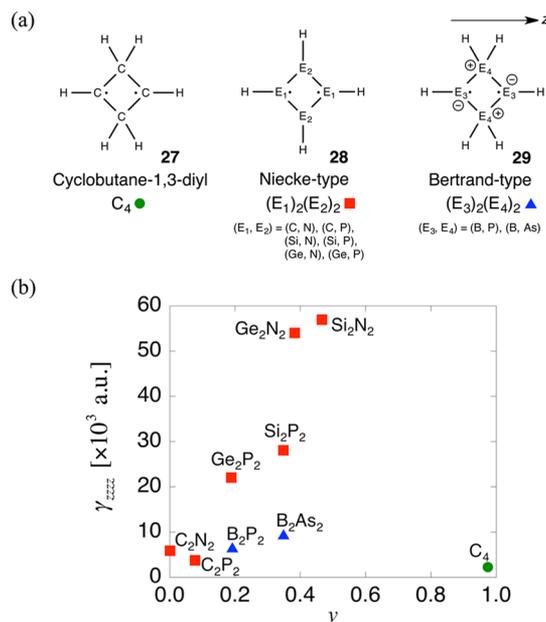


**Figure 15.** Structures of cyclobutane-1,3-diyl (**27**), Niecke-type diradicals (**28**), and Bertrand-type diradicals (**29**) (a) as well as the relationship between the diradical character ($y$) and the second hyperpolarizability $\gamma_{zzzz}$ (b), where the $y$ and $\gamma_{zzzz}$ are calculated using the LC-UBLYP($\mu$ = 0.33)/6-311++G** and UCCSD(T)/6-311++G** methods, respectively, and cyclobutane-1,3-diyl, Niecke-type, and Bertrand-type diradicals are represented by circles, squares, and triangles, respectively. Cartesian axes are also shown.

properties in traditional closed-shell molecules include the symmetric substitution by electron-donor(D) or−acceptor(A) moieties in order to achieve quadrupole-like intramolecular charge transfer (ICT). The synergy between the intermediate open-shell singlet character, the quadrupole ICT (e.g., D−$\pi$−D or A−$\pi$−A), and the $\gamma$ enhancement has been investigated using the model of $p$-quinodimethane perturbed with point charges (PQM-pc).[121] Using the UCCSD(T)/6-31G*+$p$ method, the bell-shape $y$−$\gamma$ correlation is obtained as in the case of PQM without point charges, whereas the emergence of D−$\pi$−D nature decreases the $y$ value and moves the $y$ value giving maximum $\gamma$ to the larger $y$ region as compared to the case of the PQM model. In addition, the maximum $\gamma$ value increases with the D−$\pi$−D
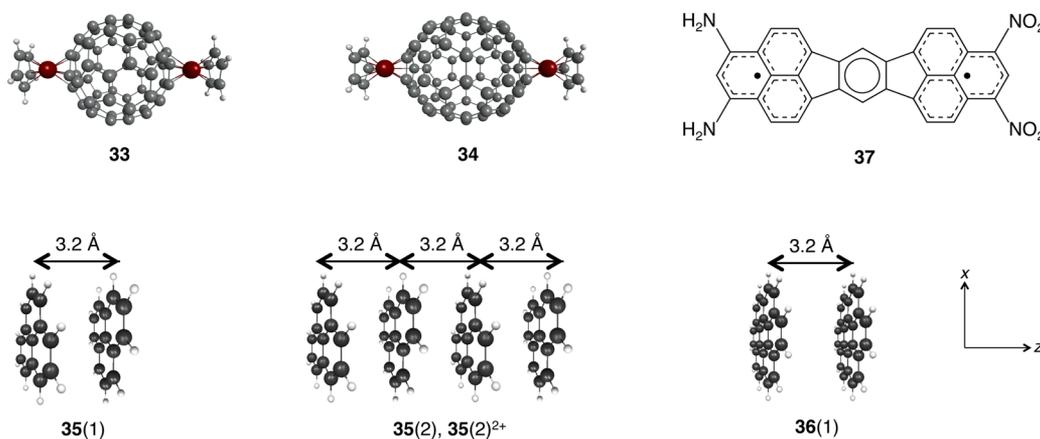
**Figure 16.** Structures of open-shell singlet systems: buckyferrocenes $(CpFe)_2\eta^5C_{60}$ (**33**) and $(CpFe)_2\eta^5C_{70}$ (**34**), one-dimensional phenalenyl clusters **35**($n$), and donor($NH_2$)/acceptor($NO_2$)-substituted IDPL (**37**) as well as of closed-shell coronene dimer (**36**(1)). Cartesian axes are also shown.

nature. These features are related to the large nonuniform charge distribution caused by the ICT in the D−π−D system.[121] From these results, we found a new design guideline for realizing efficient third-order NLO materials composed of the D−π−D or A−π−A type open-shell singlet systems: the introduction of strong D or A groups into systems with intermediate and nearly pure diradical characters enhances $\gamma$ as compared to the conventional closed-shell D−π−D or A−π−A and intermediate symmetric diradical systems with uniform charge distribution. As an example of D−π−D diradicaloid, we have investigated the $\gamma$ values of realistic Si- and Ge-disubstituted quinodimethanes.[122] It is found that the replacement of the radical sites of the originally nearly closed-shell $p$-quinodimethane framework (Figure 9) with Si (**30**) and Ge (**31**) induces an intermediate open-shell singlet nature together with a strong D−π−D type ICT, which causes an enhancement of $\gamma$ by about 1 order of magnitude as compared to that of the original $p$-quinodimethane (**32**) (see Table 1). These results are promising: the replacement radical site carbon atoms by heavy main group elements induces ICT and increases the open-shell singlet nature, which synergetically contribute to further enhancement of $\gamma$ as compared to those of closed-shell ICT systems and conventional intermediate diradicaloids without ICT nature.[121] Another example of diradicaloids with A−π−A type ICT is observed in buckyferrocenes $(CpFe)_2\eta^5C_{60}$ (**33**) and $(CpFe)_2\eta^5C_{70}$ (**34**) (Figure 16 and Table 1), which present intermediate diradical characters and, thus, large $\gamma_{zzzz}$ values comparable to those of IDPL **3**(1).[113]

*Extended Metal Atomic Chains and Open-Shell Singlet Aggregates.* As shown by the hydrogen chain studies,[84] larger size PAHs[$X,Y$],[85] one-dimensional phenalenyl radical aggregates,[88] and transition-metal atom chains (EMACs)[89] have the potential of exhibiting multiradical effects on $\gamma$ and on its size dependences, where the $\gamma$ values are enhanced in the region with intermediate multiple diradical characters $y_i$ (concerning the HOMO − $i$ and LUMO + $i$).[50] In general, the π-conjugation extension causes a decrease of the HOMO−LUMO gaps and, thus, increases the $y_i$ values. Because intermediate $y_i$ values contribute to the enhancement of the corresponding $\gamma$ and the $\gamma$ values are proportional to $R_{BA}^4$, it is important to design extended π-conjugated systems with a large number of intermediate $y_i$ values, that is, intermediate multiradical systems. To this end, tuning the intermediate orbital interaction between radical units is essential, which are realized by modifying the combination of fused-ring shapes such as five- and six-membered rings in 1D condensed-

ring chains, and by tuning the metal atom species and the interatomic distances in the EMACs. On the other hand, such control of the interunit interactions, that is, multiple diradical characters, can also be realized by adapting the intermolecular distances and configurations in aggregates or crystals. Indeed, for 1D π−π stacked phenalenyl radical aggregates **35** (Figure 16 and Table 1), the multiple diradical character strongly depends on the intermolecular distance: for a dimer close to equilibrium stacking distance, $y$ is intermediate and its $\gamma$ (in the stacking direction) is maximized. Its value per monomer exhibits about a 30-fold enhancement with respect to the isolated phenalenyl monomer.[88] This suggests that equilibrium distance is an optimum compromise between localization and delocalization of the radical electron pairs in such pancake bonding. No such effect was observed for the closed-shell coronene dimer **36**(1). Moreover, going from the dimer (diradical) to the tetramer (tetraradical), the $\gamma$ enhancement ratio increases nonlinearly with the aggregate size whereas switching from the singlet to the highest spin (quintet) state causes a significant reduction of $\gamma$ by a factor of ∼50.[88] In addition, for the tetramer, another one-order enhancement of $\gamma$ is achieved for the dicationic singlet **35**(2)$^{2+}$ in comparison to its singlet neutral state.[88] These results demonstrate the key role of intermolecular π−π stacking interactions and charge in open-shell (supra)molecular systems to achieve enhanced third-order NLO properties.

In this Perspective, design guidelines toward open-shell singlet molecular systems exhibiting remarkable nonlinear optical (NLO) responses are derived based on a two-site diradical model within the valence configuration interaction scheme. In this scheme, the concept of diradical character ($y$), a chemical index describing the bond weakness in the electronic ground state, enables to classify singlet molecular systems into three categories: (i) closed-shell ($y = 0$), (ii) intermediate diradical ($0 < y < 1$), and (iii) pure open-shell ($y = 1$) systems. Within the 2e-VCI scheme, the molecular properties (excitation energies, transition dipoles, dipole moments, second hyperpolarizabilities) of the four electronic states are expressed as a function of the diradical character, which turns out to be useful for understanding photochemical properties as well as for deducing structure−property relationships in open-shell molecular systems. It is indeed demonstrated that the second hyperpolarizability is enhanced in the intermediate diradical character region with respect to the other ones. This principle is also found to be extended to the first hyperpolarizability $\beta$ for asymmetric open-shell singlet systems. These results lead to a new class of

open-shell singlet NLO systems, which are expected to outstrip traditional closed-shell NLO systems. On the basis of this principle, practical molecular design guidelines for tuning the diradical characters and therefore for achieving large NLO properties are discussed on the basis of first-principles calculations performed on with realistic open-shell singlet molecular systems. These are substantiated by the recent synthesis of thermally stable open-shell singlet systems exhibiting large third-order NLO properties such as two-photon absorption cross sections. Besides large responses, these compounds are also good NLO switch candidates, of which the properties can be triggered by external stimuli.[123] For example, switching from the singlet to the highest spin states leads to drastic reduction of the hyperpolarizabilities, which opens the way for designing compounds with magnetic control of the NLO properties or spin states sensors.[58,61] Among strategies to achieve intermediate diradical characters, some have been demonstrated to be more efficient to achieve large $\gamma$ responses: (i) introducing asymmetricity by donor/acceptor substitution or external static field application,[124] (ii) enlarging the size of the compounds by controlling the edges topology, (iii) replacing radical site carbon atoms by heavy main group elements,[72,122] (iv) building supramolecular systems with tuned pancake bondings and specific chemical doping,[88] and (v) creating onedimensional chains of transition metal atoms.[89] These open-shell singlet systems are also interesting from the viewpoint of multifunctionality, owing to their magnetic interactions or halfmetallicity, that is, spin-dependent electric conductivity.[125]

## AUTHOR INFORMATION

**Corresponding Author**
*E-mail: mnaka@cheng.es.osaka-u.ac.jp.

**Notes**
The authors declare no competing financial interest.

**Biographies**

**Masayoshi Nakano** received his B.S. (1986), M.S. (1988), and Ph.D. (1991) degrees from Osaka University, and since 2005, he has been serving as Professor at the Department of Materials Engineering Science, Graduate School of Engineering Science, Osaka University. His research interests include quantum chemical study on the structure and function of open-shell molecular systems including nonlinear optical properties, exciton dynamics, and singlet fission. http://www.cheng.es.osaka-u.ac.jp/nakano/english/index.html

**Benoît Champagne** received his B.S. (1987), M.S. (1989), and Ph.D. (1992) degrees from Namur University. After being research fellow of the FNRS for 20 years, he was appointed Associate Professor (2009) then Full Professor (2012) in the Chemistry Department of Namur University. His research activities include the development and application of quantum chemistry methods to design molecules, polymers, and solids for NLO as well as to simulate and interpret vibrational spectra. http://www.unamur.be/sciences/chimie/ucpts/lct/

## ACKNOWLEDGMENTS

## REFERENCES

(1) Burland, D. Optical Nonlinearities In Chemistry: Introduction. *Chem. Rev.* **1994**, *94*, 1−278.
(2) *Nonlinear Optics of Organic Molecules and Polymers*; Nalwa, H. S., Miyata, S., Eds.; CRC Press: Boca Raton, FL, 1997.
(3) *Handbook of Advanced Electronic and Photonic Materials and Devices 9*; Nalwa, H. S., Ed.; Academic Press: New York, 2001.
(4) *Non-linear Optical Properties of Matter - From Molecules to Condensed Phases*; Papadopoulos, M. G., Sadlej, A. J., Leszczynski, J., Eds.; Springer: Dordrecht, The Netherlands, 2006.
(5) Parthenopoulos, D. A.; Rentzepis, P. M. Three-Dimensional Optical Storage Memory. *Science* **1989**, *245*, 843−845.
(6) Albota, M. A.; Beljonne, D.; Brédas, J. L.; Ehrlich, J. E.; Fu, J. Y.; Heikal, A. A.; Hess, S.; Kogej, T.; Levin, M. D.; Marder, S. R.; et al. Design of Organic Molecules with Large Two-Photon Absorption Cross Sections. *Science* **1998**, *281*, 1653−1656.
(7) Spangler, C. W. Recent Development in the Design of Organic Materials for Optical Power Limiting. *J. Mater. Chem.* **1999**, *9*, 2013−2020.
(8) Cumpston, B. H.; Ananthavel, S. P.; Barlow, S.; Dyer, D. L.; Ehrlich, J. E.; Erskine, L. L.; Heikal, A. A.; Kuebler, S. M.; Lee, I.-Y. S.; McCord-Maughon, D. J.; et al. Two-Photon Polymerization Initiators for Three-Dimensional Optical Data Storage and Microfabrication. *Nature* **1999**, *398*, 51−54.
(9) Kawata, S.; Sun, H.-B.; Tanaka, T.; Takada, K. Finer Features for Functional Microdevices. *Nature* **2001**, *412*, 697−698.
(10) Zhou, W.; Kuebler, S. M.; Braun, K. L.; Yu, T.; Cammack, J. K.; Ober, C. K.; Perry, J. W.; Marder, S. R. An Efficient Two-Photon-Generated Photoacid Applied to Positive-Tone 3D Microfabrication. *Science* **2002**, *296*, 1106−1109.
(11) Dichtel, W. R.; Serin, J. M.; Edder, C.; Fréchet, J. M. J.; Matuszewski, M.; Tan, L.-S.; Ohulchanskyy, T. Y.; Prasad, P. N. Singlet Oxygen Generation via Two-Photon Excited FRET. *J. Am. Chem. Soc.* **2004**, *126*, 5380−5381.
(12) He, G. S.; Tan, L.-S.; Zheng, Q.; Prasad, P. N. Multiphoton Absorbing Materials: Molecular Designs, Characterizations, and Applications. *Chem. Rev.* **2008**, *108*, 1245−1330.
(13) Terenziani, F.; Katan, C.; Badaeva, E.; Tretiak, S.; Blanchard-Desce, M. Enhanced Two-Photon Absorption of Organic Chromophores: Theoretical and Experimental Assessments. *Adv. Mater.* **2008**, *20*, 4641−4678.
(14) Pawlicki, M.; Collins, H. A.; Denning, R. G.; Anderson, H. L. Two-Photon Absorption and the Design of Two-Photon Dyes. *Angew. Chem., Int. Ed.* **2009**, *48*, 3244−3266.

(15) Dalton, L. R.; Sullivan, P. A.; Bale, D. H. Electric Field Poled Organic Electro-Optic Materials: State of the Art and Future Prospects. *Chem. Rev.* **2010**, *110*, 25–55.

(16) Slepkov, A. D.; Hegmann, F. A.; Eisler, S.; Elliott, E.; Tykwinski, R. R. The Surprising Nonlinear Optical Properties of Conjugated Polyyne Oligomers. *J. Chem. Phys.* **2004**, *120*, 6807–6810.

(17) Rumi, M.; Ehrlich, J. E.; Heikal, A. A.; Perry, J. W.; Barlow, S.; Hu, Z.; McCord-Maughon, D.; Parker, T. C.; Röckel, H.; Thayumanavan, S.; et al. Structure-property Relationships for Two-Photon Absorbing Chromophores: Bis-Donor Diphenylpolyene and Bis(styryl)benzene Derivatives. *J. Am. Chem. Soc.* **2000**, *122*, 9500–9510.

(18) Ventelon, L.; Charier, S.; Moreaux, L.; Mertz, J.; Blanchard-Desce, M. Nanoscale Push − Push Dihydrophenanthrene Derivatives as Novel Fluorophores for Two-Photon-Excited Fluorescence. *Angew. Chem., Int. Ed.* **2001**, *40*, 2098–2101.

(19) Johnston, M. D.; Subbaswamy, K. R.; Senatore, G. Hyperpolarizabilities of Alkali Halide Crystals using the Local-Density Approximation. *Phys. Rev. B: Condens. Matter Mater. Phys.* **1987**, *36*, 9202–9211.

(20) Salem, L.; Rowland, C. The Electronic Properties of Diradicals. *Angew. Chem., Int. Ed. Engl.* **1972**, *11*, 92–111.

(21) *Diradicals*; Borden, W. T., Ed.; Wiley: New York, 1982.

(22) Bonačić-Koutecký, V.; Koutecký, J.; Michl, J. Neutral and Charged Biradicals, Zwitterions, Funnels in $S_1$, and Proton Translocation: Their Role in Photochemistry, Photophysics, and Vision. *Angew. Chem., Int. Ed. Engl.* **1987**, *26*, 170–189.

(23) Rajca, A. Organic Diradicals and Polyradicals: From Spin Coupling to Magnetism? *Chem. Rev.* **1994**, *94*, 871–893.

(24) Breher, F. Stretching Bonds in Main Group Element Compounds—Borderlines between Biradicals and Closed-Shell Species. *Coord. Chem. Rev.* **2007**, *251*, 1007–1043.

(25) Lambert, C. Towards Polycyclic Aromatic Hydrocarbons with a Singlet Open-Shell Ground State. *Angew. Chem., Int. Ed.* **2011**, *50*, 1756–1758.

(26) Sun, Z.; Wu, J. Open-Shell Polycyclic Aromatic Hydrocarbons. *J. Mater. Chem.* **2012**, *22*, 4151–4160.

(27) Sun, Z.; Ye, Q.; Chi, C.; Wu, J. Low Band Gap Polycyclic Hydrocarbons: From Closed-Shell Near Infrared Dyes and Semiconductors to Open-Shell Radicals. *Chem. Soc. Rev.* **2012**, *41*, 7857–7889.

(28) Sun, Z.; Zeng, Z.; Wu, J. Benzenoid Polycyclic Hydrocarbons with an Open−Shell Biradical Ground State. *Chem. - Asian J.* **2013**, *8*, 2894–2904.

(29) Abe, M. Diradicals. *Chem. Rev.* **2013**, *113*, 7011–7088.

(30) Sun, Z.; Zeng, Z.; Wu, J. Zethrenes, Extended *p*-Quinodimethanes, and Periacenes with a Singlet Biradical Ground State. *Acc. Chem. Res.* **2014**, *47*, 2582–2591.

(31) Yamaguchi, K. In *Self-Consistent Field: Theory and Applications*; Carbo, R., Klobukowski, M., Eds.; Elsevier: Amsterdam, The Netherlands, 1990; pp 727–828.

(32) Nakano, M. *Excitation Energies and Properties of Open-Shell Singlet Molecules: Applications to a New Class of Molecules for Nonlinear Optics and Singlet Fission*; Springer: Heidelberg, Germany, 2014.

(33) Kubo, T.; Shimizu, A.; Sakamoto, M.; Uruichi, M.; Yakushi, K.; Nakano, M.; Shiomi, D.; Sato, K.; Takui, T.; Morita, Y.; et al. Synthesis, Intermolecular Interaction, and Semiconductive Behavior of a Delocalized Singlet Biradical Hydrocarbon. *Angew. Chem., Int. Ed.* **2005**, *44*, 6564–6568.

(34) Kubo, T.; Shimizu, A.; Uruichi, M.; Yakushi, K.; Nakano, M.; Shiomi, D.; Sato, K.; Takui, T.; Morita, Y.; Nakasuji, K. Singlet Biradical Character of Phenalenyl-Based Kekulé Hydrocarbon with Naphthoquinoid Structure. *Org. Lett.* **2007**, *9*, 81–84.

(35) Nishino, M.; Yamanaka, S.; Yoshioka, Y.; Yamaguchi, K. Theoretical Approaches to Direct Exchange Couplings between Divalent Chromium Ions in Naked Dimers, Tetramers, and Clusters. *J. Phys. Chem. A* **1997**, *101*, 705–712.

(36) Roos, B. O.; Borin, A. C.; Gagliardi, L. Reaching the Maximum Multiplicity of the Covalent Chemical Bond. *Angew. Chem., Int. Ed.* **2007**, *46*, 1469–1472.

(37) Cotton, F. A.; Murillo, C. A.; Zhou, H.-C. A Dichromium(II,II) Compound with a Strong Antiferromagnetic Coupling but Little or No Cr−Cr Bonding. *Inorg. Chem.* **2000**, *39*, 3728–3730.

(38) Konishi, A.; Hirao, Y.; Nakano, M.; Shimizu, A.; Botek, E.; Champagne, B.; Shiomi, D.; Sato, K.; Takui, T.; Matsumoto, K.; et al. Synthesis and Characterization of Teranthene: A Singlet Biradical Polycyclic Aromatic Hydrocarbon Having Kekulé Structures. *J. Am. Chem. Soc.* **2010**, *132*, 11021–11023.

(39) Konishi, A.; Hirao, Y.; Matsumoto, K.; Kurata, H.; Kishi, R.; Shigeta, Y.; Nakano, M.; Tokunaga, K.; Kamada, K.; Kubo, T. Synthesis and Characterization of Quarteranthene: Elucidating the Characteristics of the Edge State of Graphene Nanoribbons at the Molecular Level. *J. Am. Chem. Soc.* **2013**, *135*, 1430–1437.

(40) Nozawa, T.; Nagata, M.; Ichinohe, M.; Sekiguchi, A. Isolable p- and m-[($^t$Bu$_2$MeSi)$_2$Si]$_2$C$_6$H$_4$: Disilaquionodimethane vs Triplet Bis(silyl radical). *J. Am. Chem. Soc.* **2011**, *133*, 5773–5775.

(41) Takeuchi, K.; Ichinohe, M.; Sekiguchi, A. Access to a Stable Si$_2$N$_2$ Four-Membered Ring with Non-Kekulé Singlet Biradical Character from a Disilyne. *J. Am. Chem. Soc.* **2011**, *133*, 12478–12481.

(42) Ito, S.; Ueta, Y.; Ngo, T. T. T.; Kobayashi, M.; Hashizume, D.; Nishida, J.; Yamashita, Y.; Mikami, K. Direct Arylations for Study of the Air-Stable P-Heterocyclic Biradical: From Wide Electronic Tuning to Characterization of the Localized Radicalic Electrons. *J. Am. Chem. Soc.* **2013**, *135*, 17610–17616.

(43) Bendikov, M.; Duong, H. M.; Starkey, K.; Houk, K. N.; Carter, E. A.; Wudl, F. Oligoacenes: Theoretical Prediction of Open-Shell Singlet Diradical Ground States. *J. Am. Chem. Soc.* **2004**, *126*, 7416–7417. ibid. Addition/Correction, 2004, *126*, 10493–10493.

(44) Hachmann, J.; Dorando, J. J.; Avilés, M.; Chan, G. K.-L. The Radical Character of the Acenes: A Density Matrix Renormalization. *J. Chem. Phys.* **2007**, *127*, 134309–1–9.

(45) Casanova, D.; Head-Gordon, M. Restricted Active Space Spin-Flip Configuration Interaction Approach: Theory, Implementation and Examples. *Phys. Chem. Chem. Phys.* **2009**, *11*, 9779–9790.

(46) Tian, Y.-H.; Kertesz, M. Is There a Lower Limit to the CC Bonding Distances in Neutral Radical $\pi$-Dimers? The Case of Phenalenyl Derivatives. *J. Am. Chem. Soc.* **2010**, *132*, 10648–10649.

(47) Hayes, E. F.; Siu, A. K. Q. Electronic Structure of the Open Forms of Three-Membered Rings. *J. Am. Chem. Soc.* **1971**, *93*, 2090–2091.

(48) Yamaguchi, K. The Electronic Structures of Biradicals in the Unrestricted Hartree-Fock Approximation. *Chem. Phys. Lett.* **1975**, *33*, 330–335.

(49) Head-Gordon, M. Characterizing Unpaired Electrons from the One-Particle Density Matrix. *Chem. Phys. Lett.* **2003**, *372*, 508–511.

(50) Nakano, M.; Fukui, H.; Minami, T.; Yoneda, K.; Shigeta, Y.; Kishi, R.; Champagne, B.; Botek, E.; Kubo, T.; Ohta, K.; et al. *Theor. Chem. Acc.* **2011**, *130*, 711–724. erratum **2011**, *130*, 725.

(51) Kamada, K.; Ohta, K.; Shimizu, A.; Kubo, T.; Kishi, R.; Takahashi, H.; Botek, E.; Champagne, B.; Nakano, M. Singlet Diradical Character from Experiment. *J. Phys. Chem. Lett.* **2010**, *1*, 937–940.

(52) Calzado, C. J.; Cabrero, J.; Malrieu, J. P.; Caballol, R. Analysis of the Magnetic Coupling in Binuclear Complexes. I. Physics of the Coupling. *J. Chem. Phys.* **2002**, *116*, 2728–2747.

(53) Nakano, M.; Kishi, R.; Ohta, S.; Takahashi, H.; Kubo, T.; Kamada, K.; Ohta, K.; Botek, E.; Champagne, B. Relationship between Third-Order Nonlinear Optical Properties and Magnetic Interactions in Open-Shell Systems: A New Paradigm for Nonlinear Optics. *Phys. Rev. Lett.* **2007**, *99*, 033001–1–4.

(54) Minami, T.; Ito, S.; Nakano, M. Signature of Singlet Open-Shell Character on the Optically Allowed Singlet Excitation Energy and Singlet−Triplet Energy Gap. *J. Phys. Chem. A* **2013**, *117*, 2000–2006.

(55) Nakano, M.; Kishi, R.; Nitta, T.; Kubo, T.; Nakasuji, K.; Kamada, K.; Ohta, S.; Botek, E.; Champagne, B. Second Hyperpolarizability ($\gamma$) of Singlet Diradical Systems: Dependence of $\gamma$ on the Diradical Character. *J. Phys. Chem. A* **2005**, *109*, 885–891.

(56) Nakano, M.; Nagao, H.; Yamaguchi, K. Many-Electron Hyperpolarizability Density Analysis: Application to Dissociation Process of One-Dimensional H$_2$. *Phys. Rev. A: At., Mol, Opt. Phys.* **1997**, *55*, 1503–1513.

(57) Nakano, M.; Kishi, R.; Ohta, S.; Takebe, A.; Takahashi, H.; Furukawa, S.; Kubo, T.; Morita, Y.; Nakasuji, K.; Yamaguchi, K.; et al. Origin of the Enhancement of the Second Hyperpolarizability of Singlet Diradical Systems with Intermediate Diradical Character. *J. Chem. Phys.* **2006**, *125*, 074113−1−9.

(58) Nakano, M.; Kishi, R.; Nakagawa, N.; Ohta, S.; Takahashi, H.; Furukawa, S.; Kamada, K.; Ohta, K.; Champagne, B.; Botek, E.; et al. Second Hyperpolarizabilities ($\gamma$) of Bisimidazole and Bistriazole Benzenes: Diradical Character, Charged State and Spin State Dependences. *J. Phys. Chem. A* **2006**, *110*, 4238−4243.

(59) Nakano, M.; Kubo, T.; Kamada, K.; Ohta, K.; Kishi, R.; Ohta, S.; Nakagawa, N.; Takahashi, H.; Furukawa, S.; Morita, Y.; et al. Second Hyperpolarizabilities of Polycyclic Aromatic Hydrocarbons Involving Phenalenyl Radical Units. *Chem. Phys. Lett.* **2006**, *418*, 142−147.

(60) Nakano, M.; Nakagawa, N.; Kishi, R.; Ohta, S.; Nate, M.; Takahashi, H.; Kubo, T.; Kamada, K.; Ohta, K.; Champagne, B.; et al. Second Hyperpolarizabilities of Singlet Polycyclic Diphenalenyl Radicals: Effects of the Nature of the Central Heterocyclic Ring and Substitution to Diphenalenyl Rings. *J. Phys. Chem. A* **2007**, *111*, 9102−9110.

(61) Ohta, S.; Nakano, M.; Kubo, T.; Kamada, K.; Ohta, K.; Kishi, R.; Nakagawa, N.; Champagne, B.; Botek, E.; Takebe, A.; et al. Theoretical Study on the Second Hyperpolarizabilities of Phenalenyl Radical Systems Involving Acetylene and Vinylene Linkers: Diradical Character and Spin Multiplicity Dependences. *J. Phys. Chem. A* **2007**, *111*, 3633−3641.

(62) Nakano, M.; Nagai, H.; Fukui, H.; Yoneda, K.; Kishi, R.; Takahashi, H.; Shimizu, A.; Kubo, T.; Kamada, K.; Ohta, K.; et al. Theoretical Study of Third-Order Nonlinear Optical Properties in Square Nanographenes with Open-Shell Singlet Ground States. *Chem. Phys. Lett.* **2008**, *467*, 120−125.

(63) Nagai, H.; Nakano, M.; Yoneda, K.; Fukui, H.; Minami, T.; Bonness, S.; Kishi, R.; Takahashi, H.; Kubo, T.; Kamada, K.; et al. Theoretical Study on Third-Order Nonlinear Optical Properties in Hexagonal Graphene Nanoflakes: Edge Shape Effect. *Chem. Phys. Lett.* **2009**, *477*, 355−359.

(64) Yoneda, K.; Nakano, M.; Kishi, R.; Takahashi, H.; Shimizu, A.; Kubo, T.; Kamada, K.; Ohta, K.; Champagne, B.; Botek, E. Third-Order Nonlinear Optical Properties of Trigonal, Rhombic and Bow-Tie Graphene Nanoflakes with Strong Structural Dependence of Diradical Character. *Chem. Phys. Lett.* **2009**, *480*, 278−283.

(65) Yoneda, K.; Nakano, M.; Inoue, Y.; Inui, T.; Fukuda, K.; Shigeta, Y.; Kubo, T.; Champagne, B. Impact of Antidot Structure on the Multiradical Characters, Aromaticities and Third-Order Nonlinear Optical Properties of Hexagonal Graphene Nanoflakes. *J. Phys. Chem. C* **2012**, *116*, 17787−17795.

(66) Fukui, H.; Kishi, R.; Minami, T.; Nagai, H.; Takahashi, H.; Kubo, T.; Kamada, K.; Ohta, K.; Champagne, B.; Botek, E.; et al. Theoretical Study on Second Hyperpolarizabilities of Singlet Diradical Square Planar Nickel Complexes Involving o-Semiquinonato Type Ligands. *J. Phys. Chem. A* **2008**, *112*, 8423−8429.

(67) Fukui, H.; Nakano, M.; Shigeta, Y.; Champagne, B. Origin of the Enhancement of the Second Hyperpolarizabilities in Open-Shell Singlet Transition Metal Systems with Metal−Metal Multiple Bonds. *J. Phys. Chem. Lett.* **2011**, *2*, 2063−2066.

(68) Fukui, H.; Inoue, Y.; Yamada, T.; Ito, S.; Shigeta, Y.; Kishi, R.; Champagne, B.; Nakano, M. Enhancement of the Third-Order Nonlinear Optical Properties in Open-Shell Singlet Transition-Metal Dinuclear Systems: Effects of the Group, of the Period, and of the Charge of the Metal Atom. *J. Phys. Chem. A* **2012**, *116*, 5501−5509.

(69) Kishi, R.; Dennis, M.; Fukuda, K.; Murata, Y.; Morita, K.; Uenaka, H.; Nakano, M. Theoretical Study on the Electronic Structure and Third-Order Nonlinear Optical Properties of Open-Shell Quinoidal Oligothiophenes. *J. Phys. Chem. C* **2013**, *117*, 21498−21508.

(70) Matsui, H.; Fukuda, K.; Hirosaki, Y.; Takamuku, S.; Champagne, B.; Nakano, M. Theoretical Study on the Diradical Characters and Third-Order Nonlinear Optical Properties of Cyclic Thiazyl Diradical Compounds. *Chem. Phys. Lett.* **2013**, *585*, 112−116.

(71) Kishi, R.; Murata, Y.; Saito, M.; Morita, K.; Abe, M.; Nakano, M. Theoretical Study on Diradical Characters and Nonlinear Optical Properties of 1,3-Diradical Compounds. *J. Phys. Chem. A* **2014**, *118*, 10837−10848.

(72) Matsui, H.; Fukuda, K.; Takamuku, S.; Sekiguchi, A.; Nakano, M. Theoretical Study on the Relationship between Diradical Character and Second Hyperpolarizabilities of Four-Membered-Ring Diradicals Involving Heavy Main Group Elements. *Chem. - Eur. J.* **2015**, *21*, 2157−2164.

(73) Okuno, K.; Shigeta, Y.; Kishi, R.; Nakano, M. Photochromic Switching of Diradical Character: Design of Efficient Nonlinear Optical Switches. *J. Phys. Chem. Lett.* **2013**, *4*, 2418−2422.

(74) Kamada, K.; Ohta, K.; Kubo, T.; Shimizu, A.; Morita, Y.; Nakasuji, K.; Kishi, R.; Ohta, S.; Furukawa, S.; Takahashi, H.; et al. Strong Two-Photon Absorption of Singlet Diradical Hydrocarbons. *Angew. Chem., Int. Ed.* **2007**, *46*, 3544−3546.

(75) Ishida, M.; Shin, J.-Y.; Lim, J. M.; Lee, B. S.; Yoon, M.-C.; Koide, T.; Sessler, J. L.; Osuka, A.; Kim, D. Neutral Radical and Singlet Biradical Forms of Meso-Free, -Keto, and -Diketo Hexaphyrins(1.1.1.1.1.1): Effects on Aromaticity and Photophysical Properties. *J. Am. Chem. Soc.* **2011**, *133*, 15533−15544.

(76) Zeng, Z.; Sung, Y. M.; Bao, N.; Tan, D.; Lee, R.; Zafra, J. L.; Lee, B. S.; Ishida, M.; Ding, J.; Navarrete, J. T. L.; et al. Stable Tetrabenzo-Chichibabin's Hydrocarbons: Tunable Ground State and Unusual Transition between Their Closed-Shell and Open-Shell Resonance Forms. *J. Am. Chem. Soc.* **2012**, *134*, 14513−14525.

(77) Li, Y.; Heng, W.-K.; Lee, B. S.; Aratani, N.; Zafra, J. L.; Bao, N.; Lee, R.; Sung, Y. M.; Sun, Z.; Huang, K.-W.; et al. Kinetically Blocked Stable Heptazethrene and Octazethrene: Closed-Shell or Open-Shell in the Ground State? *J. Am. Chem. Soc.* **2012**, *134*, 14913−14922.

(78) Kamada, K.; Fuku-en, S.-I.; Minamide, S.; Ohta, K.; Kishi, R.; Nakano, M.; Matsuzaki, M.; Okamoto, H.; Higashikawa, H.; Inoue, K.; et al. Impact of Diradical Character on Two-Photon Absorption: Bis(acridine) Dimers Synthesized from an Allenic Precursor. *J. Am. Chem. Soc.* **2013**, *135*, 232−241.

(79) Zeng, Z.; Ishida, M.; Zafra, J. L.; Zhu, X.; Sung, Y. M.; Bao, N.; Webster, R. D.; Lee, B. S.; Li, R.-W.; Zeng, W.; et al. Pushing Extended $\pi$-Quinodimethanes to the Limit: Stable Tetracyano-Oligo(N-Annulated Perylene)Quinodimethanes with Tunable Ground States. *J. Am. Chem. Soc.* **2013**, *135*, 6363−6371.

(80) Sun, Z.; Lee, S.; Park, K. H.; Zhu, X.; Zhang, W.; Zheng, B.; Hu, P.; Zeng, Z.; Das, S.; Li, Y.; et al. Dibenzoheptazethrene Isomers with Different Biradical Characters: An Exercise of Clar's Aromatic Sextet Rule in Singlet Biradicaloids. *J. Am. Chem. Soc.* **2013**, *135*, 18229−18236.

(81) Das, S.; Lee, S.; Son, M.; Zhu, X.; Zhang, W.; Zheng, B.; Hu, P.; Zeng, Z.; Sun, Z.; Zeng, W.; et al. para-Quinodimethane-Bridged Perylene Dimers and Pericondensed Quaterrylenes: The Effect of the Fusion Mode on the Ground States and Physical Properties. *Chem. - Eur. J.* **2014**, *20*, 11410−11420.

(82) Kishida, H.; Hibino, K.; Nakamura, A.; Kato, D.; Abe, J. Third-Order Nonlinear Optical Properties of a $\pi$-Conjugated Biradical Molecule Investigated by Third-Harmonic Generation Spectroscopy. *Thin Solid Films* **2010**, *519*, 1028−1030.

(83) Takauji, K.; Suizu, R.; Awaga, K.; Kishida, H.; Nakamura, A. Third-Order Nonlinear Optical Properties and Electroabsorption Spectra of an Organic Biradical, [Naphtho[2,1-d:6,5-d']bis([1,2,3]-dithiazole)]. *J. Phys. Chem. C* **2014**, *118*, 4303−4308.

(84) Nakano, M.; Takebe, A.; Kishi, R.; Ohta, S.; Nate, M.; Kubo, T.; Kamada, K.; Ohta, K.; Champagne, B.; Botek, E.; et al. Second Hyperpolarizabilities ($\gamma$) of Open-Shell Singlet One-Dimensional Systems: Intersite Interaction Effects on the Average Diradical Character and Size Dependences of $\gamma$. *Chem. Phys. Lett.* **2006**, *432*, 473−479.

(85) Nagai, H.; Nakano, M.; Yoneda, K.; Kishi, R.; Takahashi, H.; Shimizu, A.; Kubo, T.; Kamada, K.; Ohta, K.; Botek, E.; Chanpagne, B. Signature of Multiradical Character in Second Hyperpolarizabilities of Rectangular Graphene Nanoflakes. *Chem. Phys. Lett.* **2010**, *489*, 212−218.

(86) Yoneda, K.; Nakano, M.; Fukui, H.; Minami, T.; Shigeta, Y.; Kubo, T.; Botek, E.; Champagne, B. Open-Shell Characters and Second Hyperpolarizabilities of One-Dimensional Graphene Nanoflakes Composed of Trigonal Graphene Units. *ChemPhysChem* **2011**, *12*, 1697−1707.

(87) Nakano, M.; Minami, T.; Fukui, H.; Kishi, R.; Shigeta, Y.; Champagne, B. Full Configuration Interaction Calculations of the Second Hyperpolarizabilities of the $H_4$ Model Compound: Summation-Over-States Analysis and Interplay with Diradical Characters. *J. Chem. Phys.* **2012**, *136*, 024315−1−7.

(88) Yoneda, K.; Nakano, M.; Fukuda, K.; Matsui, H.; Takamuku, S.; Hirosaki, Y.; Kubo, T.; Kamada, K.; Champagne, B. Third-Order Nonlinear Optical Properties of One-Dimensional Open-Shell Molecular Aggregates Composed of Phenalenyl Radicals. *Chem. - Eur. J.* **2014**, *20*, 11129−11136.

(89) Fukui, H.; Takamuku, S.; Yamada, T.; Fukuda, K.; Takebayashi, T.; Shigeta, Y.; Kishi, R.; Champagne, B.; Nakano, M. Open-Shell Character and Second Hyperpolarizabilities of One-Dimensional Chromium(II) Chains: Size Dependence and Bond-Length Alternation Effect. *Inorg. Chem.* **2014**, *53*, 8700−8707.

(90) Nakano, M.; Champagne, B. Diradical Character Dependences of the First and Second Hyperpolarizabilities of Asymmetric Open-Shell Singlet Systems. *J. Chem. Phys.* **2013**, *138*, 244306−1−13.

(91) Nakano, M.; Champagne, B.; Botek, E.; Ohta, K.; Kamada, K.; Kubo, T. Giant Electric Field Effect on the Second Hyperpolarizability of Symmetric Singlet Diradical Molecules. *J. Chem. Phys.* **2010**, *133*, 154302−1−15.

(92) Yoneda, K.; Nakano, M.; Fukuda, K.; Champagne, B. The Odd Electron Density Is the Guide toward Achieving Organic Molecules with Gigantic Third-Order Nonlinear Optical Responses. *J. Phys. Chem. Lett.* **2012**, *3*, 3338−3342.

(93) Nakano, M.; Yoneda, K.; Kishi, R.; Takahashi, H.; Kubo, T.; Kamada, K.; Ohta, K.; Botek, E.; Champagne, B. Remarkable Two-Photon Absorption in Open-Shell Singlet Systems. *J. Chem. Phys.* **2009**, *131*, 114316−1−7.

(94) Heisenberg, W. Zur Theorie des Ferromagnetismus. *Eur. Phys. J. A* **1928**, *49*, 619−636.

(95) Orr, B. J.; Ward, J. F. Perturbation Theory of the Non-Linear Optical Polarization of an Isolated System. *Mol. Phys.* **1971**, *20*, 513−526.

(96) Bishop, D. M. Explicit Nondivergent Formulas for Atomic and Molecular Dynamic Hyperpolarizabilities. *J. Chem. Phys.* **1994**, *100*, 6535−6542.

(97) Nakano, M.; Yamaguchi, K. A Proposal of New Organic Third-Order Nonlinear Optical Compounds. Centrosymmetric Systems with Large Negative Third-Order Hyperpolarizabilities. *Chem. Phys. Lett.* **1993**, *206*, 285−292.

(98) Nakano, M.; Shigemoto, I.; Yamada, S.; Yamaguchi, K. Size-Consistent Approach and Density Analysis of Hyperpolarizability: Second Hyperpolarizabilities of Polymeric Systems with and without Defects. *J. Chem. Phys.* **1995**, *103*, 4175−4191.

(99) Ohta, K.; Kamada, K. Theoretical Investigation of Two-Photon Absorption Allowed Excited States in Symmetrically Substituted Diacetylenes by Ab Initio Molecular-Orbital Method. *J. Chem. Phys.* **2006**, *124*, 124303−1−11.

(100) Kamada, K.; Ohta, K.; Iwase, Y.; Kondo, K. Two-Photon Absorption Properties of Symmetric Substituted Diacetylene: Drastic Enhancement of the Cross Section near the One-Photon Absorption Peak. *Chem. Phys. Lett.* **2003**, *372*, 386−393.

(101) Perez-Moreno, J.; Clays, K.; Kuzyk, M. G. A New Dipole-Free Sum-Over-States Expression for the Second Hyperpolarizability. *J. Chem. Phys.* **2008**, *128*, 084109−1−11.

(102) Nakano, M.; Champagne, B. Diradical Character Dependence of Third-Harmonic Generation Spectra in Open-Shell Singlet Systems. *Theor. Chem. Acc.* **2015**, *134*, 23−1−9.

(103) Toto, J. L.; Toto, T. T.; de Melo, C. P.; Hasan, M.; Kirtman, B. Ab Initio Finite Oligomer Method for Nonlinear Optical Properties of Conjugated Polymers. Effect of Electron Correlation on the Static Longitudinal Hyperpolarizability of Polyacetylene. *Chem. Phys. Lett.* **1995**, *244*, 59−64.

(104) Dalskov, E. K.; Oddershede, J.; Bishop, D. M. Static and Dynamic Polarizability Calculations for the Polyyne Series $(C_{2n}H_2)$ with Extrapolation to the Infinite Chain. *J. Chem. Phys.* **1998**, *108*, 2152−2161.

(105) Shuai, Z.; Brédas, J. L. Coupled-Cluster Approach for Studying the Electronic and Nonlinear Optical Properties of Conjugated Molecules. *Phys. Rev. B: Condens. Matter Mater. Phys.* **2000**, *62*, 15452−15460.

(106) Schulz, M.; Tretiak, S.; Chernyak, V.; Mukamel, S. Size Scaling of Third-Order Off-Resonant Polarizabilities. Electronic Coherence in Organic Oligomers. *J. Am. Chem. Soc.* **2000**, *122*, 452−459.

(107) de A. Machado, A. E.; Petrov, D. V.; Falcao, E. H. L.; da Gama, A. A. S.; de Azevedo, W. M. Semiempirical Calculations of Aniline Oligomers Hyperpolarisabilities. *Chem. Phys. Lett.* **2002**, *356*, 451−456.

(108) Moore, E. E.; Yaron, D. Theoretical Studies Concerning the Optimization of Conjugated Molecules for Third-Order Nonlinear Optics. *J. Phys. Chem. A* **2002**, *106*, 5339−5347.

(109) Champagne, B.; Mosley, D. H. Electron Correlation Effects on the Static Longitudinal Second Hyperpolarizability of Polymeric Chains. Møller−Plesset Perturbation Theory Investigation of Hydrogen Model Chains. *J. Chem. Phys.* **1996**, *105*, 3592−3603.

(110) Nakano, M.; Yamada, S.; Yamaguchi, K. Hyperpolarizabilities of One-Dimensional H*n* Systems: Second Hyperpolarizability Density Analyses for Regular and Charged Solitonlike Linear Chains. *Int. J. Quantum Chem.* **1998**, *70*, 269−282.

(111) Nakano, M.; Kishi, R.; Takebe, A.; Nate, M.; Takahashi, H.; Kubo, T.; Kamada, K.; Ohta, K.; Champagne, B.; Botek, E. Second Hyperpolarizability of Zethrenes. *Comput. Lett.* **2007**, *3*, 333−338.

(112) Muhammad, S.; Fukuda, K.; Minami, T.; Kishi, R.; Shigeta, Y.; Nakano, M. Interplay between Diradical Characters and Third-Order Nonlinear Optical Properties in Fullerene Systems. *Chem. - Eur. J.* **2013**, *19*, 1677−1685.

(113) Muhammad, S.; Ito, S.; Nakano, M.; Kishi, R.; Yoneda, K.; Kitagawa, Y.; Shkir, M.; Irfan, A.; Chaudhry, A. R.; AlFaify, S.; Kalam, A.; Al-Sehemi, A. G. Diradical Character and Nonlinear Optical Properties of Buckyferrocenes: Focusing on the Use of Suitably Modified Fullerene Fragments. *Phys. Chem. Chem. Phys.* **2015**, *17*, 5805−5816.

(114) Kishi, R.; Bonness, S.; Yoneda, K.; Takahashi, H.; Nakano, M.; Botek, E.; Champagne, B.; Kubo, T.; Kamada, K.; Ohta, K.; et al. Long-Range Corrected Density Functional Theory Study on Static Second Hyperpolarizabilities of Singlet Diradical Systems. *J. Chem. Phys.* **2010**, *132*, 094107−1−11.

(115) Clar, E. *Polycyclic Hydrocarbons*; Academic Press: London, 1964.

(116) Nakano, M.; Nitta, T.; Yamaguchi, K.; Champagne, B.; Botek, E. Spin Multiplicity Effects on the Second Hyperpolarizability of an Open-Shell Neutral π-Conjugated System. *J. Phys. Chem. A* **2004**, *108*, 4105−4111.

(117) Motomura, S.; Nakano, M.; Fukui, H.; Yoneda, K.; Kubo, T.; Carion, R.; Champagne, B. Size Dependences Of The Diradical Character And The Second Hyperpolarizabilities In Dicyclopenta-Fused Acenes: Relationships With Their Aromaticity/Antiaromaticity. *Phys. Chem. Chem. Phys.* **2011**, *13*, 20575−20583.

(118) Roos, B. O.; Borin, A. C.; Gagliardi, L. Reaching the Maximum Multiplicity of the Covalent Chemical Bond. *Angew. Chem., Int. Ed.* **2007**, *46*, 1469−1472.

(119) Inoue, Y.; Yamada, T.; Champagne, B.; Nakano, M. Equatorial Ligand Effects on the Diradical Character Dependence of the Second Hyperpolarizabilities of Open-Shell Singlet Transition-Metal Dinuclear Complexes. *Chem. Phys. Lett.* **2013**, *570*, 75−79.

(120) Yamada, T.; Takamuku, S.; Matsui, H.; Champagne, B.; Nakano, M. Axial Ligand Effects on the Diradical Characters and Second Hyperpolarizabilities of Open-Shell Singlet Transition-Metal Dinuclear Complexes. *Chem. Phys. Lett.* **2014**, *608*, 68−73.

(121) Fukuda, K.; Nakano, M. Intramolecular Charge Transfer Effects on the Diradical Character and Second Hyperpolarizabilities of Open-Shell Singlet X−π−X (X = Donor/Acceptor) Systems. *J. Phys. Chem. A* **2014**, *118*, 3463−3471.

(122) Fukuda, K.; Nozawa, T.; Yotsuyanagi, H.; Ichinohe, M.; Sekiguchi, A.; Nakano, M. Theoretical Study on the Enhancement of the Second Hyperpolarizabilities of Si-, Ge-Disubstituted Quinodimethanes: Synergy Effects of Open-Shell Nature and Intramolecular Charge Transfer. *J. Phys. Chem. C* **2015**, *119*, 1188−1193.

(123) Castet, F.; Rodriguez, V.; Pozzo, J. L.; Ducasse, L.; Plaquet, A.; Champagne, B. Design and Characterization of Molecular Nonlinear Optical Switches. *Acc. Chem. Res.* **2013**, *46*, 2656−2665.

(124) Nakano, M.; Minami, T.; Yoneda, K.; Muhammad, S.; Kishi, R.; Shigeta, Y.; Kubo, T.; Rougier, L.; Champagne, B.; Kamada, K.; et al. Giant Enhancement of the Second Hyperpolarizabilities of Open-Shell Singlet Polyaromatic Diphenalenyl Diradicaloids by an External Electric Field and Donor-Acceptor Substitution. *J. Phys. Chem. Lett.* **2011**, *2*, 1094−1098.

(125) Son, Y.-W.; Cohen, M. L.; Louie, S. G. Half-Metallic Graphene Nanoribbons. *Nature* **2006**, *444*, 347−349.